

# Systematically smaller single-epoch quasar black hole masses using a radius-luminosity relationship corrected for spectral bias

Jaya Maithil,<sup>1\*</sup> Michael S. Brotherton,<sup>1</sup> Ohad Shemmer,<sup>2</sup> Pu Du,<sup>3</sup> Jian-Min Wang,<sup>3,4,5</sup>  
Adam D. Myers,<sup>1</sup> Jacob N. McLane,<sup>1</sup> Cooper Dix,<sup>2</sup> and Brandon M. Matthews<sup>2</sup>

<sup>1</sup>*Department of Physics and Astronomy, University of Wyoming, Laramie, WY 82071, USA*

<sup>2</sup>*Department of Physics, University of North Texas, Denton, TX 76203, USA*

<sup>3</sup>*Key Laboratory for Particle Astrophysics, Institute of High Energy Physics, Chinese Academy of Sciences, 19B Yuquan Road, Beijing 100049, People's Republic of China*

<sup>4</sup>*National Astronomical Observatories of China, Chinese Academy of Sciences, 20A Datun Road, Beijing 100020, People's Republic of China*

<sup>5</sup>*School of Astronomy and Space Science, University of Chinese Academy of Sciences, 19A Yuquan Road, Beijing 100049, People's Republic of China*

Accepted 2022 June 17. Received 2022 June 16; in original form 2021 May 1

## ABSTRACT

Determining black hole masses and accretion rates with better accuracy and precision is crucial for understanding quasars as a population. These are fundamental physical properties that underpin models of active galactic nuclei. A primary technique to measure the black hole mass employs the reverberation mapping of low-redshift quasars, which is then extended via the radius-luminosity relationship for the broad-line region to estimate masses based on single-epoch spectra. An updated radius-luminosity relationship incorporates the flux ratio of optical Fe II to H $\beta$  ( $\equiv \mathcal{R}_{\text{Fe}}$ ) to correct for a bias in which more highly accreting systems have smaller line-emitting regions than previously realized. In this current work, we demonstrate and quantify the effect of using this Fe-corrected radius-luminosity relationship on mass estimation by employing archival data sets possessing rest-frame optical spectra over a wide range of redshifts. We find that failure to use a Fe-corrected radius predictor results in overestimated single-epoch black hole masses for the most highly accreting quasars. Their accretion rate measures ( $L_{\text{Bol}}/L_{\text{Edd}}$  and  $\dot{M}$ ), are similarly underestimated. The strongest Fe-emitting quasars belong to two classes: high- $z$  quasars with rest-frame optical spectra, which given their extremely high luminosities, require high accretion rates, and their low- $z$  analogs, which given their low black holes masses, must have high accretion rates to meet survey flux limits. These classes have mass corrections downward of about a factor of two, on average. These results strengthen the association of the dominant Eigenvector 1 parameter  $\mathcal{R}_{\text{Fe}}$  with the accretion process.

**Key words:** galaxies: active - quasars: supermassive black holes

## 1 INTRODUCTION

Black hole mass and accretion rate are arguably the two most important properties of quasars. They are vital in understanding the growth of supermassive black holes and how feedback from quasars regulates the growth of massive galaxies. In the past decade, more than 50 quasars have been discovered at  $z > 6$  that are claimed to have billion solar mass black holes (e.g., Mortlock et al. 2011; Wang et al. 2021). Such findings challenge our understanding of black hole formation and growth. To form a billion solar mass black hole when the universe was  $\leq 1$  Gyr old requires a massive seed black hole,  $M_{\text{seed}} \geq 10^3 M_{\odot}$ , in an Eddington-limited accretion rate scenario

(e.g., Lodato & Natarajan 2006; Johnson et al. 2012). Alternatively, accretion with reduced radiative efficiency,  $\epsilon = 0.01 - 0.001$ , could explain the growth in such a short cosmic time (e.g., Volonteri et al. 2015; Trakhtenbrot et al. 2017; Davies et al. 2019). Another possible explanation for such apparently large quasar black hole masses at such early times could also simply be a systematic overestimation.

For nearby (distance  $< 300$  Mpc,  $z < 0.06$ ) active galactic nuclei (AGNs), direct measurement of black hole mass is made using stellar and gas dynamics (Kormendy & Ho 2013). These methods are not possible for distant objects because of limited angular resolution and the fact that quasars outshine their host galaxy. Observations of the correlated variation of the continuum and photoionized broad emission lines (especially Balmer lines) in type-I AGNs led to the development of the reverberation mapping (RM) technique

\* E-mail: jmaithil@uwyo.edu

to determine black hole masses (e.g., Peterson 1993). Time delays between the continuum and emission-line variability, derived from multiple epochs of spectroscopy, can be used to measure the size of the broad-line region (BLR) (Blandford & McKee 1982; Netzer & Peterson 1997; Peterson 1993, 2014). Combining this measurement with the emission-line velocity dispersion provides an estimate of the virialized black hole mass (see equation 1) (Peterson et al. 2004). Over the past two decades, RM has provided black hole mass measurements for over a hundred AGNs (e.g., Bentz & Katz 2015; Yu et al. 2020a). However, it is impractical to apply the RM method for every AGN as it is resource-intensive. Fortunately, RM studies show a relationship between the BLR size and the continuum luminosity to be  $R \propto L^{-0.5}$  (Kaspi et al. 2000, 2005, 2007, 2021; Bentz et al. 2006, 2009, 2013). RM studies based on the  $H\beta$  line provide the most reliable correlations (Bentz et al. 2013). Using the luminosity at  $5100\text{\AA}$  from single-epoch (SE) spectra, one can then predict the size of the BLR and estimate the black hole mass (e.g., Laor 1998; Wandel et al. 1999; Vestergaard & Peterson 2006).

For the highest redshift quasars, most of the optical-UV lines fall in the near-infrared part of the spectrum, for which there are fewer spectral observations. The masses of the black holes that power high-redshift quasars are therefore estimated using UV continuum luminosities and emission lines like C IV and Mg II, calibrated against  $H\beta$  RM measurements, a procedure that introduces additional uncertainties. The offset between Mg II or C IV-based black hole masses with  $H\beta$ -based masses is in part related to Eigenvector 1 (EV1) spectral trends (e.g., Shen et al. 2008; Runnoe et al. 2013b; Brotherton et al. 2015) that appear to be correlated with Eddington ratio (Boroson & Green 1992; Boroson 2002; Yuan & Wills 2003; Marziani et al. 2001; Shen & Ho 2014; Sun & Shen 2015). Shen et al. (2008) demonstrated that the offset between Mg II and C IV-based SE black hole mass correlates with another EV1 parameter, C IV blueshift. Runnoe et al. (2013b) identified a similar bias in C IV-based masses using the ratio of C IV to the  $\lambda 1400$  feature (a blend of Si IV + O IV). Brotherton et al. (2015) demonstrated that an EV1 bias in reverberation-mapped AGN samples that leads to a 50% overestimation of C IV-based masses in average quasars. Recent results from Dalla Bontà et al. (2020) show that the difference between C IV-based RM masses and SE masses anti-correlates with Eddington ratio.

The  $H\beta$  RM sample originally used to establish the R-L relationship primarily included objects with strong narrow [O III] emission lines. This is because [O III] lines are convenient for relative flux calibration (van Groningen & Wanders 1992) and such objects also tend to have strong broad  $H\beta$  line variability. The equivalent width (EW) of [O III] is anti-correlated with the Eddington ratio ( $L_{\text{bol}}/L_{\text{Edd}}$ , described in Section 2) (Boroson & Green 1992; Marziani et al. 2001; Boroson 2002; Shen & Ho 2014), hence, RM samples were biased toward low-accretion-rate broad-lined AGNs (i.e., Eddington ratio of a few to a few tens of percent). Recent  $H\beta$  RM campaigns, such as the Super-Eddington Accreting Massive Black Hole (SEAMBH; Du et al. 2014, 2016, 2018) and the Sloan Digital Sky Survey Reverberation Mapping projects (SDSS-RM; Shen et al. 2015) find deviations from the canonical R-L relationship. The observed time lags are sometimes significantly smaller than predicted (Du et al. 2015, 2016; Grier et al. 2017; Du et al. 2018; Du & Wang 2019). The offsets in the  $H\beta$  SDSS-RM sample are not due to observational bias, but rather they reflect the wide variety of broad-line radii occupied by AGNs (Fonseca Alvarez et al. 2020). Moreover, the offset between the observed and predicted BLR radius shows an anti-correlation with the EV1 accretion rate parameters (Du et al. 2018; Du & Wang 2019; Dalla Bontà et al.

2020). Even the Mg II and C IV RM samples demonstrate similar offsets in BLR radius that are correlated with accretion rate parameters, suggesting that current R-L relationships should include some additional correction terms (Martínez-Aldama et al. 2020; Dalla Bontà et al. 2020).

The SEAMBH  $H\beta$  RM sample comprises a population of highly accreting AGNs with a BLR radius up to 3-8 times smaller than predicted from the canonical R-L relationship, which implies an overestimation of SE black hole masses by the same factor. The SEAMBH RM results also establish a strong anti-correlation between the deviation from the canonical R-L relationship and the relative strength of Fe II, an EV1 parameter that correlates with the Eddington ratio. Using a sample of 75 RM AGNs, Du & Wang (2019) updated and tightened the R-L relationship by introducing the relative strength of Fe II as a predictive parameter. Yu et al. (2020a) provide a similar accretion-rate-based correction to the R-L relation using the strength of Fe II. Such a correction should be extremely significant for luminous high-redshift quasars, which are likely to be accreting at a high rate. Using the Eddington ratio distribution for a uniformly selected sample of type 1 quasars from SDSS DR7, Kelly & Shen (2013) employed a flexible Bayesian technique to demonstrate that the fraction of quasars with a higher Eddington ratio becomes larger at high redshift. Therefore, the canonical R-L relationship most likely overestimates the masses of the black holes hosted by high-redshift quasars. Similarly, the dimensionless accretion rate parameter ( $\dot{M}$ ) and Eddington ratio, which are inversely proportional to black hole mass, are likely to be underestimated. Even this underestimated  $\dot{M}$  results in a large population of super-Eddington quasars,  $\dot{M} > 3$ , which necessitates the use of an accretion rate corrected R-L relationship (see Figure 5 in Section 4).

This paper adopts the Du & Wang (2019) R-L relationship to quantify this effect using archival data of low and high-redshift quasars. Our results demonstrate that for objects with large  $\mathcal{R}_{\text{Fe}}$ , the SE method adopting the canonical R-L relation significantly overestimates their  $H\beta$ -based masses and underestimates their accretion rates by factors of a couple to several. In section 2, we explain the method to determine black hole mass and accretion rate parameters with the new and canonical R-L relationship. Section 3 describes the low and high redshift samples used and summarizes the quantities used to estimate black hole mass. We discuss our results regarding the black hole mass and accretion rate in section 4.1 and the correlation between  $\mathcal{R}_{\text{Fe}}$  and accretion rate parameters in section 4.2, followed by additional discussion and conclusions in sections 5 and 6, respectively. Throughout the paper, we adopt a cosmology with  $H_0 = 70 \text{ km s}^{-1} \text{ Mpc}^{-1}$ ,  $\Omega_\Lambda = 0.7$  and  $\Omega_m = 0.3$ .

## 2 BLACK HOLE MASS AND ACCRETION RATE

Black hole masses ( $M_{\text{BH}}$ ) are estimated using the following relationship

$$M_{\text{BH}} = f \left( \frac{R_{\text{BLR}} \Delta V^2}{G} \right). \quad (1)$$

This equation assumes the virialized motion of BLR clouds under the gravitational potential of the central black hole (e.g., Wandel et al. 1999; Peterson et al. 2004). The expression in parenthesis is called virial product. The full-width at half maximum (FWHM) or line dispersion ( $\sigma_{\text{line}}$ ) of broad emission lines like  $H\beta$  sets the velocity ( $\Delta V$ ) assuming Doppler broadening. The size of the BLR,  $R_{\text{BLR}}$ , can then be determined by multiplying the time lag ( $\Delta\tau$ ) between

emission-line and continuum variability, determined by reverberation mapping, by the speed of light ( $R_{\text{BLR}} = c\Delta\tau$ ). The virial coefficient,  $f$ , accounts for the unknown geometry, kinematics, and inclination of the BLR. Although its value differs from one AGN to another, a mean value of  $f$  is obtained empirically by calibrating RM mass against mass predicted by the  $M - \sigma_*$  relation seen in quiescent galaxies (Onken et al. 2004, and many others since). Here we focus on H $\beta$ -based SE virial black hole mass and adopt FWHM of H $\beta$  as the measure of  $\Delta V$ .

The monochromatic luminosity at 5100Å in  $\text{erg s}^{-1}$ ,  $\lambda L_{\lambda, 5100\text{\AA}}$  (hereafter  $L_{5100\text{\AA}}$ ), serves as a proxy for  $R_{\text{BLR}}$ . We use two R-L relationships: (1) the canonical R-L relationship established by Bentz et al. (2013)

$$\log(R_{\text{H}\beta}/\text{lt} - \text{days}) = K + \mu \log(L_{5100\text{\AA}}/10^{44} \text{ erg s}^{-1}), \quad (2)$$

where,  $K = 1.527 \pm 0.031$  &  $\mu = 0.533 \pm 0.035$ , and (2) an accretion rate corrected R-L relationship established by Du & Wang (2019)

$$\log(R_{\text{H}\beta}/\text{lt} - \text{days}) = \alpha + \beta \log \ell_{44} + \gamma \mathcal{R}_{\text{Fe}}, \quad (3)$$

where,  $\ell_{44} = L_{5100\text{\AA}}/10^{44} \text{ erg s}^{-1}$ ,  $\alpha = 1.65 \pm 0.06$ ;  $\beta = 0.45 \pm 0.03$ ;  $\gamma = -0.35 \pm 0.08$ . It takes into account the relative strength of Fe II,  $\mathcal{R}_{\text{Fe}}$ , that is known to correlate with EV1.  $\mathcal{R}_{\text{Fe}}$  is defined as the ratio of flux ( $F$ ) or rest-frame equivalent width (EW) between Fe II and H $\beta$ , i.e.,  $\mathcal{R}_{\text{Fe}} = F(\text{Fe II})/F(\text{H}\beta) \approx \text{EW}(\text{Fe II})/\text{EW}(\text{H}\beta)$ . A higher  $\mathcal{R}_{\text{Fe}}$  value leads to a systematically smaller  $R_{\text{BLR}}$  estimate and is likely associated with a higher accretion rate (Du & Wang 2019, and our discussion later in this paper).

We estimate the SE virial black hole mass by determining  $R_{\text{BLR}}$  from the R-L relationships, using FWHM of H $\beta$  as the velocity term, and a virial coefficient  $f = 1.5$  in equation 1. Our choice of the virial coefficient is consistent with the empirical mean value of  $f$  obtained by calibrating FWHM-based RM black hole mass from rms spectra with the  $M - \sigma_*$  relation. We adopted the Ho & Kim (2014) value of  $f = 1.5 \pm 0.4$  for AGNs in classical bulges and ellipticals that have black hole mass greater than  $10^7 M_{\odot}$ . Recent work by Yu et al. (2020b, 2019) also finds  $f = 1.51 \pm 0.20$  for low-redshift RM AGNs in classical bulges and ellipticals. Henceforth, we shall refer to the SE black hole mass estimated using equation 2 as the ‘‘canonical’’ black hole mass,  $M_{\text{H}\beta, \text{canonical}}$  and the one using equation 3 as the ‘‘Fe-corrected’’ black hole mass,  $M_{\text{H}\beta, \text{Fe-corrected}}$ . Note that we adopt  $f = 1.5$  for both canonical and Fe-corrected black hole mass estimates. Therefore, the  $\mathcal{R}_{\text{Fe}}$  factor in the Du & Wang (2019) R-L relationship (equation 3) dominates the difference between  $M_{\text{H}\beta, \text{canonical}}$  and  $M_{\text{H}\beta, \text{Fe-corrected}}$ .

We calculate two relative accretion rate parameters based on luminosity and black hole mass. First, there is the dimensionless accretion rate parameter,  $\dot{M}$ , derived from the Shakura & Sunyaev (1973) thin accretion disk model for which

$$\dot{M} = 20.1 (\ell_{44}/\cos i)^{3/2} m_7^{-2}, \quad (4)$$

where,  $m_7 = M_{\text{BH}}/10^7 M_{\odot}$ , and  $i$  is inclination angle to the line of sight (Wang et al. 2014b; Du et al. 2014, 2018; Du & Wang 2019). We take  $\cos i = 0.75$ , an average for type 1 AGNs, for our calculation. Second, we have the Eddington ratio, ( $L_{\text{bol}}/L_{\text{Edd}}$ ) expressed as the ratio of the bolometric luminosity ( $L_{\text{bol}}$ ) to the Eddington luminosity ( $L_{\text{Edd}} = 1.5 \times 10^{45} m_7 \text{ erg s}^{-1}$ ). We calculate  $L_{\text{bol}}$  using the Richards et al. (2006) relation,  $L_{\text{bol}} = 9.26 L_{5100\text{\AA}}$ .

$$L_{\text{bol}}/L_{\text{Edd}} = \frac{9.26 L_{5100\text{\AA}}}{1.5 \times 10^{45} m_7} \quad (5)$$

The bolometric luminosity may saturate in the case of quasars with

super-Eddington accretion owing to the photon trapping effect in their slim accretion disks (Wang et al. 1999; Mineshige et al. 2000). This, in principle, may make  $\dot{M}$  a better predictor of accretion rate, although the two are highly correlated for quasars, as we will show.

For the flux-to-luminosity conversion we use  $\lambda L_{\lambda} [\text{erg s}^{-1}] = 4 \pi D_{\text{L}}^2 f_{\lambda} (1+z)\lambda$ , where  $f_{\lambda}$  is the monochromatic flux at the rest-wavelength ( $\lambda$ ) in units of  $\text{erg s}^{-1} \text{ cm}^{-2} \text{ \AA}^{-1}$ ,  $D_{\text{L}}$  is the luminosity distance, and  $z$  is the redshift (Hogg et al. 2002).

### 3 ARCHIVAL DATA SETS AND MEASUREMENTS

To characterize the effect of using the new R-L relationship (equation 3) on H $\beta$ -based black hole mass estimates, and hence also estimates of accretion rate, we selected archival samples and associated catalogs that provide: a) flux or EW of Fe II between rest-frame 4435-4685 Å and the broad H $\beta$  component to calculate  $\mathcal{R}_{\text{Fe}}$ , b) flux or luminosity at rest-frame 5100 Å to estimate the BLR size from the new R-L relationship, and c) FWHM H $\beta$  to provide a proxy for velocity dispersion.

For low-redshift quasars ( $z < 0.7$ ), we used only the catalog of Shen et al. (2011), which is highly complete with uniform measurements of the quantities we need for objects in the Sloan Digital Sky Survey Data Release 7 (Abazajian et al. 2009, SDSS DR7). The Shen et al. (2011) catalog contains a total of 105,783 quasars. We applied a conservative S/N and redshift cutoff to obtain a sample unbiased by poor-quality spectra in the H $\beta$  region. Our selection criteria include a median S/N per pixel in the H $\beta$  region greater than 20, redshift  $z < 0.7$ , and non-zero measurements of EW and FWHM H $\beta$ . Our choice of S/N > 20 per pixel eliminates unreliable line width measurements and reduces the formal uncertainties in SE masses to a minimum (Denney et al. 2009). Given the automatic nature of spectral fits in Shen et al. (2011), some individual measurements are bad. So we applied a S/N > 3 cut on the H $\beta$  line measurements as an additional quality control check. We eliminated three targets, SDSS J094927.67+314110.0, SDSS J105528.80+312411.3, and SDSS J151036.74+510854.6 because of erroneous measurements due to incorrect redshifts<sup>1</sup>, giving a total of 3309 quasars.

Shen et al. (2011) did not correct the cataloged 5100 Å luminosities for host-galaxy contamination. We applied a correction when  $\log[L_{5100\text{\AA}}/(\text{erg s}^{-1})] < 45.053$ , using equation 1 of Shen et al. (2011). Recently, Dalla Bontà et al. (2020) defined a host-galaxy light correction based on the luminosity of the H $\beta$  line,  $L(\text{H}\beta)$ . We tested the effect of our choice of using Shen et al. (2011) host-galaxy correction method against the method described by Dalla Bontà et al. (2020) for the canonical and Fe-corrected black hole mass estimates. There is essentially no change in the mass difference distribution between the two different methods when correcting  $L_{5100\text{\AA}}$  for the low-luminosity sub-sample ( $\log[L_{5100\text{\AA}}/(\text{erg s}^{-1})] < 45.0$ ). The mean mass differences are 0.14 dex with the Shen et al. correction, 0.13 dex with the Dalla Bontà et al. correction, and the standard deviations are 0.19 dex and 0.18 dex, respectively. There are systematic differences in the host-galaxy correction method defined by Dalla Bontà et al. and Shen et al.. On average, Dalla Bontà et al. method underestimates  $L_{5100\text{\AA}}$  by a factor of 1.28 compared to Shen et al. method. For highly luminous quasars ( $\log[L_{5100\text{\AA}}/(\text{erg s}^{-1})] > 45.0$ ), the mean underestimation

<sup>1</sup> While inspecting the SDSS spectrum of outliers in Figure 7, 8 & 9, these three quasars had wrong redshifts assigned to them.

**Table 1.** Data sets used in our analysis

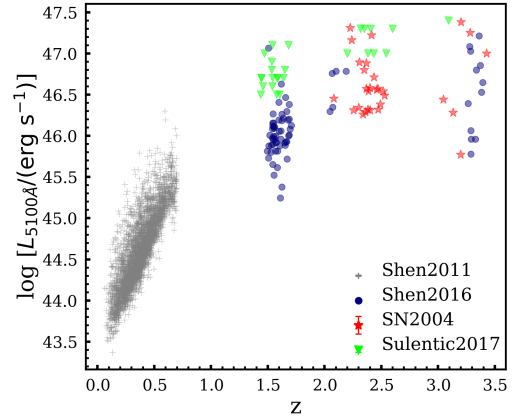
Ref	Sample	Sample size	Redshift
Shen et al. (2011)	Shen2011	3309	< 0.7
Shen (2016)	Shen2016	71	1.5-3.5
Shemmer et al. (2004), Netzer et al. (2004)	SN2004	29	2-3.5
Sulentic et al. (2017)	Sulentic2017	26	1.4-3.1

in  $L_{5100\text{\AA}}$  by Dalla Bontà et al. method is a factor of 1.32 compared to Shen et al., with 40% of quasars underestimated by a factor of 1.32-13.18. Note that the Shen et al. method is not sensitive to any host galaxy emission when the spectral absorption features disappear; hence this method underestimates the host-galaxy correction for the most luminous quasars. Even though the Dalla Bontà et al.  $L(\text{H}\beta)$ - $L_{5100\text{\AA}}$  correlation is relatively tight, it is based on a small sample, and there may be issues extrapolating to higher  $L_{5100\text{\AA}}$ . There is an additional concern that EW  $\text{H}\beta$  correlates with  $\mathcal{R}_{\text{Fe}}$  ( $P < 1\%$ ; Boroson & Green (1992)) and using an  $L_{5100\text{\AA}}$  based on  $L(\text{H}\beta)$  might bias Fe-corrected black hole mass estimates.

For high-redshift quasars, the  $\text{H}\beta$  region falls in the near-infrared (IR). A good signal-to-noise (S/N) near-IR spectrum of a low-luminosity high-redshift quasar requires an exorbitantly large amount of observing time on most telescopes. As a result, archival samples at high redshift predominantly contain high-luminosity quasars. Only a handful of samples tabulate the Fe II measurement essential for our study. Our analysis includes all the high-redshift samples we found that provide good spectral measurements required to calculate canonical and Fe-corrected black hole mass. These high-redshift samples are a near-IR follow-up of quasars with previous rest-frame UV spectral observation selecting targets based primarily on two criteria: 1) high S/N ratio in the spectral region containing UV emission lines like C IV and N V and 2) redshifts for which  $\text{H}\beta$  falls in unobscured near-IR spectral bands (i.e., JHK bands). Appendix A provides more detailed information about the individual sample selection of the high-redshift samples from the work of Shen (2016), the two-part series by Shemmer et al. (2004) & Netzer et al. (2004) (hereafter SN2004), and Sulentic et al. (2017).

Table 1 lists the name of the samples we use, their total number of objects, and their redshift range. Shen (2016) contains 74 quasars in the redshift range  $1.5 \leq z \leq 3.5$ . We eliminated one quasar, J0810+0936, with a strangely large uncertainty reported for its luminosity measurement ( $\log [L_{5100\text{\AA}}/(\text{erg s}^{-1})] = 46.30 \pm 23.16$ ). Shen (2016) report rest-frame EWs, which we used to calculate  $\mathcal{R}_{\text{Fe}}$ , and include 71 quasars with  $\mathcal{R}_{\text{Fe}} < 3$ . SN2004 consists of 29 quasars in the redshift range  $2 \leq z \leq 3.5$ . We used the tabulated systemic redshift,  $5100\text{\AA}$  luminosity and best-fit FWHM  $\text{H}\beta$  values from Shemmer et al. (2004), and  $\mathcal{R}_{\text{Fe}}$  measurements given by Netzer et al. (2004). Sulentic et al. (2017) catalog the properties of a sample of 28 quasars with  $1.4 \leq z \leq 3.1$ , including two weak-line quasars (HE0359-3959, HE2352-4010) that we eliminate for our analysis<sup>2</sup>. We used their tabulated  $\mathcal{R}_{\text{Fe}}$  measurements and FWHM  $\text{H}\beta$  of the broad component obtained from the spectral fit analysis. Our final combined sample provides redshift coverage  $0.05 < z < 3.6$  and represents a typical range of luminosity seen in low and high-redshift quasars (Figure 1).

We calculated  $M_{\text{H}\beta, \text{canonical}}$  for all samples by using the canon-

**Figure 1.** Redshift vs  $L_{5100\text{\AA}}$ . The plot shows the redshift-luminosity space spanned by our quasar samples.

ical R-L relation (equation 2), with FWHM  $\text{H}\beta$  as a proxy for the velocity, and  $f = 1.5$  in equation 1. All of these literature sources except Sulentic et al. (2017) provide EWs, and use the EW ratio as  $\mathcal{R}_{\text{Fe}}$ . Netzer et al. (2004) mention that the flux ratio is the same as the EW ratio used to define  $\mathcal{R}_{\text{Fe}}$  by Boroson & Green (1992). Sulentic et al. (2017) use line flux ratios to calculate  $\mathcal{R}_{\text{Fe}}$ , and note that this is equivalent to using EW ratios. We used the Du & Wang (2019) R-L relation (equation 3), with FWHM  $\text{H}\beta$  as a proxy for the velocity and  $f = 1.5$  in equation 1, to calculate  $M_{\text{H}\beta, \text{Fe-corrected}}$  for each sample. For Shen et al. (2011) quasars, we used the luminosity corrected for host-galaxy contamination to estimate both  $M_{\text{H}\beta, \text{canonical}}$  and  $M_{\text{H}\beta, \text{Fe-corrected}}$ .

For Shen et al. (2011) and Shen (2016) samples, we propagated the measurement uncertainties in FWHM  $\text{H}\beta$ ,  $L_{5100\text{\AA}}$ , EW  $\text{H}\beta$  and EW Fe II to calculate the error in the derived quantities like  $\mathcal{R}_{\text{Fe}}$ ,  $R_{\text{BLR}}$ ,  $M_{\text{BH}}$ ,  $L_{\text{Bol}}/L_{\text{Edd}}$ , and  $\mathcal{M}$ . For other samples, we made a few assumptions to estimate measurement uncertainties. SN2004 provide the uncertainty in FWHM  $\text{H}\beta$  as the difference between direct and best-fit measures for each source and quotes an average uncertainty of 25% on  $L_{5100\text{\AA}}$ . We assumed an uncertainty of 24% for  $\mathcal{R}_{\text{Fe}}$  based on the mean uncertainty reported by McIntosh et al. (1999) with similar data quality and spectral resolution. Sulentic et al. (2017) list uncertainty in  $5100\text{\AA}$  flux but do not provide uncertainties in spectral measurements. As Sulentic et al. (2017) obtained the spectra from the parent samples of Sulentic et al. (2004, 2006) and Marziani et al. (2009) and redid the analysis; their spectral measurements are consistent but not identical. So we obtained the relative error in FWHM  $\text{H}\beta$ , EW  $\text{H}\beta$ , and EW Fe II for each target in Sulentic et al. (2017) from the parent samples to estimate uncertainties in derived quantities. Our error propagation also includes uncertainties in the virial coefficient ( $f$ ) and the coefficients in the two R-L relationships. We list the mean measurement uncertainties in the derived quantities for each sample in Table 2 and show them as typical error bars in our figures.

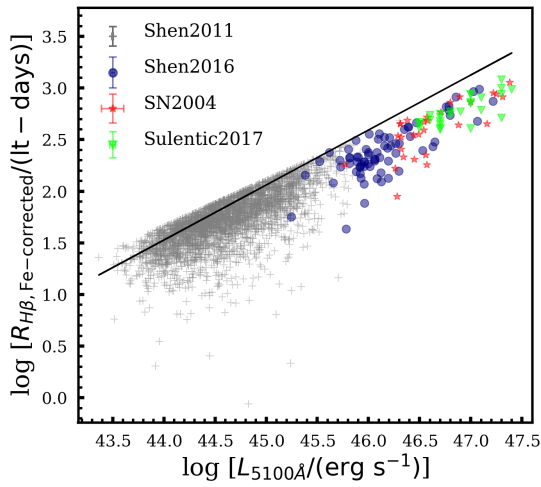
## 4 RESULTS

Figure 2 shows the Fe-corrected R-L relationship (equation 3) for all the samples. For the luminous high- $z$  quasars with strong  $\mathcal{R}_{\text{Fe}}$ , the Du & Wang (2019) R-L relation gives a smaller  $R_{\text{BLR}}$  as compared to the canonical R-L relationship (equation 2). The same effect emerges in low- $z$  quasars with strong  $\mathcal{R}_{\text{Fe}}$ . For low- $z$  quasars with

<sup>2</sup> We include the two weak-line quasars from Sulentic et al. (2017) and two others from Shemmer et al. (2010) in Appendix B

**Table 2.** Mean measurement uncertainties on the derived quantities for each sample

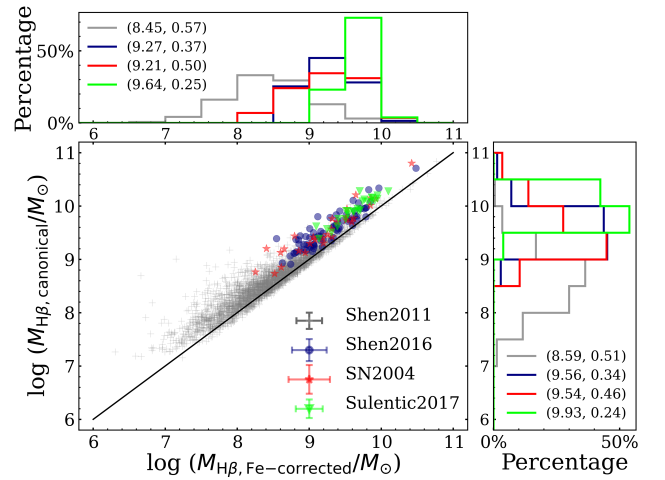
Quantities	Mean measurement error			
	Shen2011	Shen2016	SN2004	Sulentic2017
$R_{H\beta, \text{canonical}}$	0.04 dex	0.08 dex	0.11 dex	0.11 dex
$M_{H\beta, \text{canonical}}$	0.15 dex	0.20 dex	0.27 dex	0.17 dex
$L_{\text{Bol}}/L_{\text{Edd, canonical}}$	0.15 dex	0.20 dex	0.27 dex	0.17 dex
$\mathcal{M}_{\text{canonical}}$	0.30 dex	0.41 dex	0.53 dex	0.35 dex
$\mathcal{R}_{\text{Fe}}$	0.10 dex	0.15 dex	0.10 dex	0.11 dex
$R_{H\beta, \text{Fe-corrected}}$	0.10 dex	0.15 dex	0.14 dex	0.13 dex
$M_{H\beta, \text{Fe-corrected}}$	0.17 dex	0.24 dex	0.29 dex	0.19 dex
$L_{\text{Bol}}/L_{\text{Edd, Fe-corrected}}$	0.18 dex	0.24 dex	0.29 dex	0.19 dex
$\mathcal{M}_{\text{Fe-corrected}}$	0.35 dex	0.48 dex	0.57 dex	0.37 dex


**Figure 2.** Fe-corrected  $R_{\text{BLR}}$  using equation 3 vs  $5100\text{\AA}$  luminosity for our quasar samples. The black solid line represents the canonical R-L relation. It shows that the Du & Wang (2019) R-L relation predicts a smaller BLR radius than the canonical R-L relation for higher accretion rate quasars marked with strong  $\mathcal{R}_{\text{Fe}}$ .

$0 \leq \mathcal{R}_{\text{Fe}} \leq 0.42$ , the  $\mathcal{R}_{\text{Fe}}$  correction is small, and the Du & Wang (2019) R-L relation gives a larger  $R_{\text{BLR}}$  owing to the difference in zero-point and coefficient of luminosity ( $\alpha = 1.65$ ,  $\beta = 0.45$ ) compared to the canonical R-L relationship ( $K = 1.527$ ,  $\mu = 0.533$ ). These differences in the predicted  $R_{\text{BLR}}$  from the two R-L relationships propagate to their black hole mass estimates and consequently to the accretion rates.

#### 4.1 The effects of the Fe correction on mass and accretion rate

Figure 3 compares the Fe-corrected black hole masses against the canonical masses. The majority of the points (80%) lie above the 1:1 line, indicating a systematic overestimation of black hole mass when using the canonical R-L relation. Non-parametric tests such as Kolmogorov–Smirnov (K-S) test ( $p=1.84e-22$ ) and the Wilcoxon rank sum test (two-sided  $p=6.27e-25$ ) indicate that the differences in values and overall distributions between the two sets of masses significantly differ, as expected, since  $\mathcal{R}_{\text{Fe}}$  values are significantly above zero in significant fractions of the quasar population. It should be noted that the K-S and Wilcoxon rank sum tests do not take into


**Figure 3.** Black hole mass calculated using the canonical (y-axis) and Fe-corrected (x-axis) R-L relation. The histograms on top and right show the percentage distributions (i.e., the fraction of targets in each bin  $\times 100$ )

of the Fe-corrected and canonical mass, respectively. The numbers in brackets give the mean and standard deviation of each sample. The plot shows that the black hole mass is systematically overestimated using the canonical R-L relation.

account the measurement errors. We will discuss the  $\mathcal{R}_{\text{Fe}}$  distribution for our samples in Section 5.1.

The low- $z$  Shen et al. (2011) quasars have a very large range in black-hole masses,  $10^6 < M_{\text{BH}} (M_{\odot}) < 10^{11}$ . The higher redshift samples have a smaller range of black hole masses,  $10^8 < M_{\text{BH}} (M_{\odot}) < 10^{10.5}$ . Figure 3 also shows that the deviation from the 1:1 line becomes pronounced moving to the very lowest mass quasars,  $M_{\text{BH}} < 10^8 M_{\odot}$ . These low-mass quasars have larger  $\mathcal{R}_{\text{Fe}}$  and higher accretion rates (see Figures 13 & 14 in the Section 5.1) resulting in smaller Fe-corrected black hole masses. Therefore, in the low- $z$  quasars, the Fe-correction is most important for the less massive, highly accreting objects. The subplots on the right and top show the percentage of the canonical and Fe-corrected mass, respectively, for each sample and their statistical means and standard deviations. The mean of each sample shifts to a lower  $M_{\text{BH}}$  when using the Du & Wang R-L relation. Note that Shen et al. (2011) sample consists of a tiny population (20 out of 3309) of quasars with  $10^6 \leq M_{\text{BH}} (M_{\odot}) \leq 10^7$  for which  $f = 0.7 \pm 0.2$  may be more appropriate (Ho & Kim 2014, for the low mass AGNs with pseudobulges). Our choice of  $f = 1.5$  likely overestimates both the canonical and Fe-corrected black hole masses of these 20

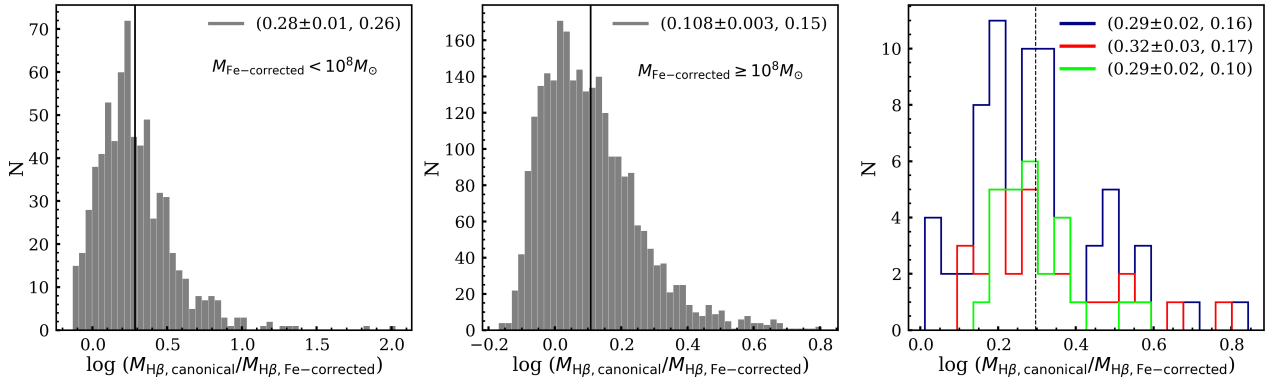


**Figure 4.** Left: Histogram of the distribution of mass ratios for the low- $z$  Shen2011 quasars with mass less than  $10^8 M_{\odot}$ . The mean  $\pm$  the standard error of the mean, and the standard deviation for each sample are given in the parentheses. The mean ratio for this low-mass sub-sample is  $0.28 \pm 0.01$ , represented by the black solid line, and the standard deviation is 0.26, as stated in parentheses. Middle: Same as left figure but for the Shen2011 quasars with mass  $\geq 10^8 M_{\odot}$ . The mean ratio for the high-mass sub-sample is  $0.108 \pm 0.003$ , represented by the black solid line, and the standard deviation is 0.15, as given in parentheses. Right: Histogram of the distribution of mass ratio for the high- $z$  samples colour-coded for each sample same as Figure 3. The individual mean and standard deviation are given in the parentheses. The mean ratio for the high- $z$  samples is  $0.30 \pm 0.01$ , represented by the black dashed line, and the standard deviation is 0.18.

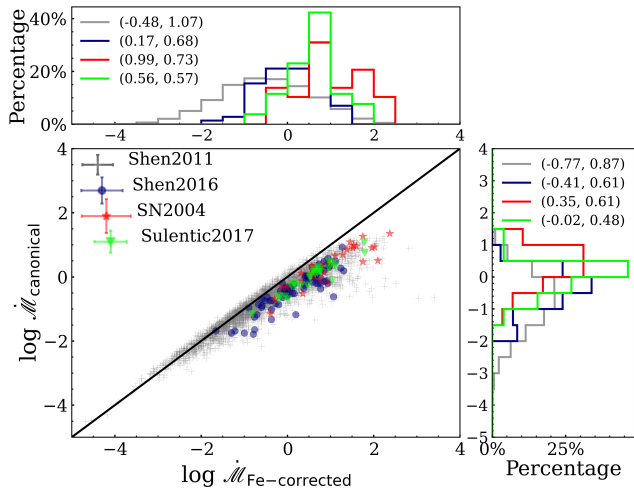


**Figure 5.** Canonical vs Fe-corrected accretion rate calculated using equation 3. It shows that the accretion rate is systematically underestimated when the canonical R-L relationship based black hole mass is used. The histograms on the right and top show the percentage distribution (i.e., the fraction of targets in each bin  $\times 100$ ) of canonical and Fe-corrected accretion rate, respectively. They show that the mean accretion rate for each sample increases when the Fe-corrected R-L relationship based mass is used.

quasars alike, although without impacting the ratio of the canonical to Fe-corrected mass.

To further illustrate the change in mass when the Fe correction is applied, we plot the distribution of the log of the ratio of canonical-to-Fe-corrected mass for the low- $z$  Shen et al. (2011) sample in the left and the middle panels of Figure 4. The left histogram consists of quasars with  $M_{\text{Fe-corrected}} < 10^8 M_{\odot}$ , whereas the middle panel shows quasars with  $M_{\text{Fe-corrected}} \geq 10^8 M_{\odot}$ . The low-mass quasars ( $< 10^8 M_{\odot}$ ), on average, have a much larger overestimation, a factor of  $\sim 2$ , compared to a factor of  $\sim 1.3$  for the high-mass ( $\geq 10^8 M_{\odot}$ ) quasars in the low- $z$  sample. The low-mass quasars are the ones with the strongest  $\mathcal{R}_{\text{Fe}}$  (see Figure 14). For the low- $z$  quasars with weaker  $\mathcal{R}_{\text{Fe}}$ , using the Du & Wang (2019) R-L relation slightly overestimates the black hole mass of  $\sim 22\%$  of the

sample compared to the canonical, owing to small differences in intercept and coefficient of luminosity.

The right histogram of Figure 4 illustrates the change in mass for samples from Table 1, which excludes Shen et al. (2011). On average, the black hole masses of these high- $z$  samples decrease by about 0.3 dex or a factor of 2, as depicted by the dotted black line. The difference is up to a factor of 2 for 60% of the sample and a factor of 2-4.7 for 37%. The mean difference in mass in Shen (2016) is a factor of  $\sim 2$ , in SN 2004 is a factor of  $\sim 2.1$ , and in Sulentic et al. (2017) is a factor of  $\sim 2$ .

Next, we calculated the dimensionless accretion rate parameter defined in equation 4 using both canonical and Fe-corrected black hole mass. The comparison between canonical and Fe-corrected  $\dot{M}$  (Figure 5) demonstrates that the accretion rates are underestimated, in agreement with the inverse relationship between  $\dot{M}$  and the black hole mass. The distribution in Figure 5 shows that the mean  $\dot{M}$  for each sample is larger for the Fe-corrected black hole mass. For low- $z$  quasars, i.e., the Shen et al. (2011) sample, the logarithm of  $\dot{M}_{\text{Fe-corrected}}$  has a mean  $\pm$  the standard error of the mean<sup>3</sup> of  $-0.48 \pm 0.02$ , and it ranges from  $-4.68$  to  $3.40$ . Whereas the high- $z$  quasars (samples other than Shen et al. 2011) have systematically higher  $\log \dot{M}_{\text{Fe-corrected}}$  values with a mean of  $0.44 \pm 0.07$  and range from  $-1.66$  to  $2.37$ . Figure 6 compares  $\dot{M}$  with the traditionally used Eddington ratio, both calculated using the Fe-corrected black hole mass. The log of the Fe-corrected Eddington ratio for the low- $z$  quasars ranges from  $-3.19$  to  $0.95$  and has a mean value of  $-1.04 \pm 0.01$ , whereas the high- $z$  quasars have a higher mean value of  $\log L_{\text{Bol}}/L_{\text{Edd,Fe-corrected}} = -0.13 \pm 0.04$  and range from  $-1.38$  to  $0.80$ .

As mentioned earlier, the canonical and Fe-corrected black hole mass differ primarily due to the  $\mathcal{R}_{\text{Fe}}$  factor, an accretion rate indicator. Therefore, the plot of the change in the black hole mass or the mass ratio exhibits the expected strong correlation with the two accretion rate parameters,  $L_{\text{Bol}}/L_{\text{Edd}}$  &  $\dot{M}$  (Figure 7). We visually inspected the SDSS spectra of the Shen et al. (2011) quasars with

<sup>3</sup> Note that the standard error of the mean quoted in the figures and text is purely statistical in nature (ratio of standard deviation and square root of sample size) and does not take into account the measurement uncertainties.

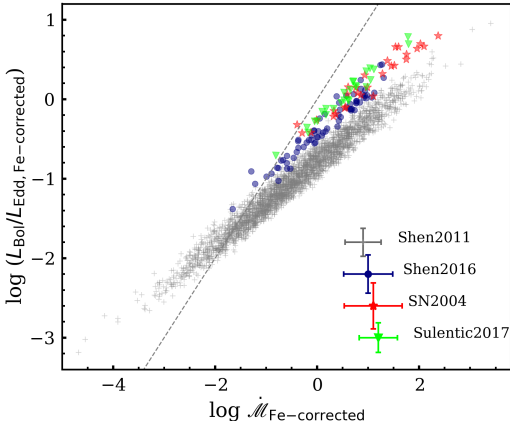


**Figure 6.** Corrected Eddington ratio vs accretion rate parameter for all samples. The grey dashed line represents the 1:1 relation for reference.

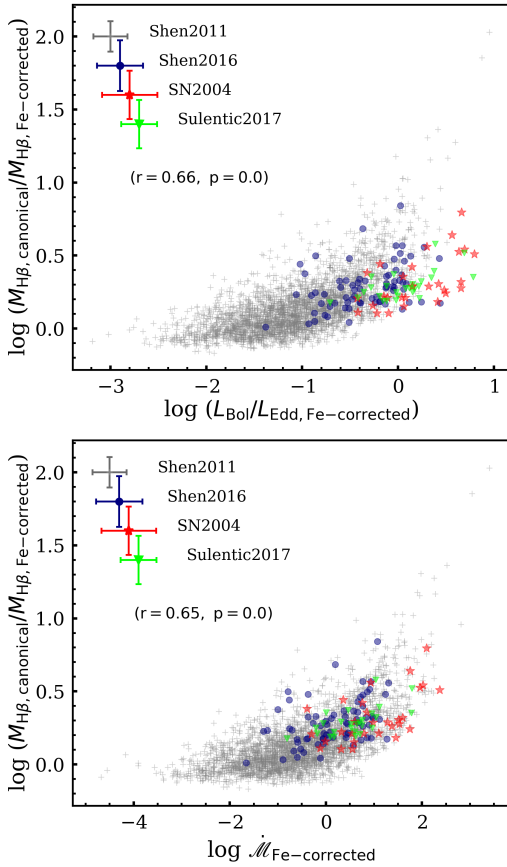


**Figure 7.** Mass ratio vs Fe-corrected Eddington ratio (top panel) and dimensionless accretion rate (bottom panel). Change in mass shows a strong correlation with the accretion rate parameters. The Pearson  $r$  coefficients for these correlations are given in parentheses.

the log of the mass ratio  $\geq 1$ , which appear as outliers in Figure 7. Their spectra are consistent with the EV1 trend of strong relative strength of Fe II (see Appendix C).

Figure 8 displays the mass ratio plotted against the Fe-corrected mass colour-coded by the Fe-corrected accretion rate. It shows the mean mass ratio in each mass bin for low and high- $z$  samples separately. The mean mass ratio and the standard error of the mean

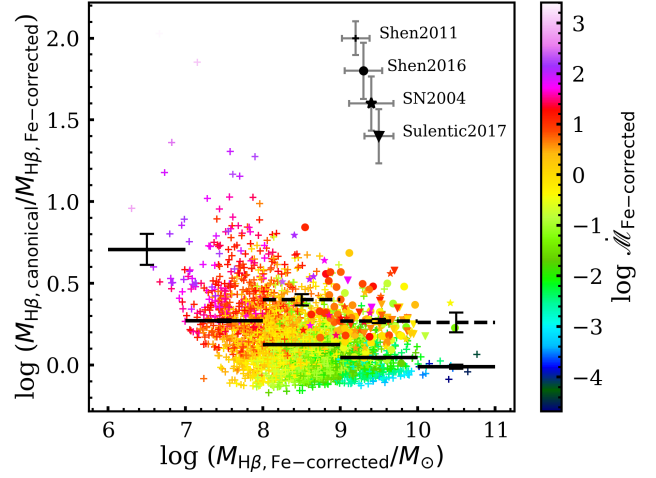


**Figure 8.** Mass ratio vs Fe-corrected black hole mass colour-coded by accretion rate. Black solid and dashed lines represent the mean mass ratio in each mass bin for the low- $z$  sample and the high- $z$  samples, respectively. The black error bars represent the standard error of the mean ratio in each mass bin. The grey error bars on the top of each sample represent the typical measurement error in the mass ratio. For  $M_{\text{H}\beta, \text{Fe-corrected}} > 10^8 M_{\odot}$ , the high- $z$  samples have a mean mass ratio greater than the low- $z$  sample.

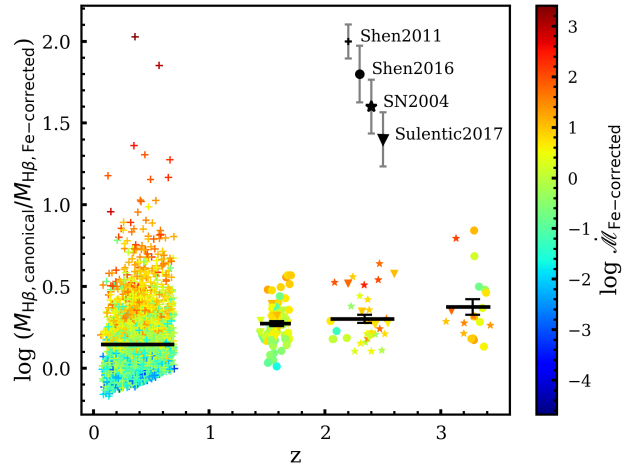


**Figure 9.** Mass ratio between canonical and Fe-corrected black hole mass vs redshift, colour-coded by accretion rate. Black solid lines show the mean mass ratio within the redshift range presented by the length of the line. Black error bars shows the standard error of the mean mass ratio. The plot shows that the difference between the canonical and Fe-corrected mass increases as the redshift increases. The mean mass ratio in redshift bins  $2 \leq z < 3$  and  $z > 3$  differ at the  $\sim 1.1\sigma$  level. On average, the high- $z$  quasars ( $z > 1$ ) have higher accretion rates.

in each mass bin for the low- $z$  sample are  $0.71 \pm 0.09$  dex in  $10^6 \leq M_{\text{BH}} (M_{\odot}) < 10^7$ ,  $0.27 \pm 0.01$  dex in  $10^7 \leq M_{\text{BH}} (M_{\odot}) < 10^8$ ,  $0.125 \pm 0.003$  dex in  $10^8 \leq M_{\text{BH}} (M_{\odot}) < 10^9$ ,  $0.045 \pm 0.004$  dex in  $10^9 \leq M_{\text{BH}} (M_{\odot}) < 10^{10}$  and  $-0.01 \pm 0.01$  dex in  $M_{\text{BH}} \geq 10^{10} M_{\odot}$ . The mean mass ratio and the standard error of mean in each mass bin for the high- $z$  samples are  $0.40 \pm 0.03$  dex in  $10^8 \leq M_{\text{BH}} (M_{\odot}) < 10^9$ ,  $0.27 \pm 0.01$  dex in  $10^9 \leq M_{\text{BH}} (M_{\odot}) < 10^{10}$  and  $0.26 \pm 0.06$  dex in  $M_{\text{BH}} \geq 10^{10} (M_{\odot})$ . Figure 8 demonstrates that the lower mass quasars ( $M_{\text{BH}} < 10^8 M_{\odot}$ ) of the low- $z$  Shen et al. (2011) sample have a higher accretion rate, hence, larger mass correction.

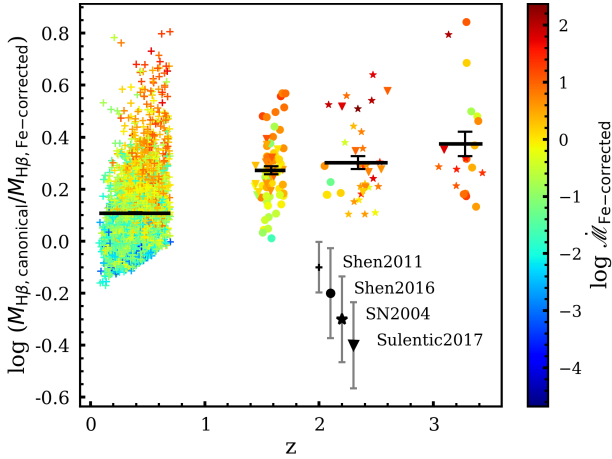


**Figure 10.** Same as Figure 9 with only  $M_{\text{H}\beta, \text{Fe-corrected}} > 10^8 M_{\odot}$  targets with  $z < 0.7$ .

For  $M_{\text{BH}} \geq 10^8 M_{\odot}$ , the mass correction is, on average, larger in the high- $z$  samples compared to the low- $z$  sample.

Plotting the change in black hole mass against redshift, colour-coded by accretion rate, Figure 9 shows that, on average, the over-estimation of mass increases as the redshift increases. The mean mass differences is  $0.145 \pm 0.003$  dex for  $z < 1$ ,  $0.27 \pm 0.01$  dex for  $1 < z < 2$ ,  $0.30 \pm 0.02$  dex for  $2 < z < 3$  and  $0.37 \pm 0.05$  dex for  $z > 3$ . Figure 9 also demonstrates that the high- $z$  ( $z > 1$ ) quasars on average have higher accretion rate black holes as compared to the low- $z$  quasars, which include a large fraction of high mass but low-accretion rate objects (also see Figure 13). It also shows that for  $z > 1$ , the fraction of high accretion rate quasars increases as redshift increases and their masses are overestimated by a factor of two to several using the canonical R-L relationship. Figures 8 & 9 show that the high- $z$  quasars have larger masses and mass correction; they also have larger accretion rates on average (see Figure 7) – the high- $z$  quasars lack quasars with very weak Fe II that are present in large numbers in the low-redshift Shen et al. (2011) sample (see Figure 14). This is likely a selection effect due to the difficulty of observing lower luminosity quasars at high- $z$ .

Figure 10 is qualitatively the same as Figure 9 but includes only  $M_{\text{BH}} > 10^8 M_{\odot}$  quasars from the low redshift Shen et al. (2011) sample. This eliminates 692 quasars with strong  $\mathcal{R}_{\text{Fe}}$  and high accretion rate, giving a mean mass difference of  $0.108 \pm 0.003$  dex for this low- $z$  sub-sample. Figure 10 demonstrates the stark difference the Fe-correction makes on the quasars with comparable black hole masses in the low and high-redshift samples.

#### 4.2 A stronger correlation between $\mathcal{R}_{\text{Fe}}$ and accretion rate parameters after using Fe-corrected mass

The dominant trend of decreasing EW[OIII] with the increasing  $\mathcal{R}_{\text{Fe}}$  is known as Eigenvector 1 (EV1) (Boroson & Green 1992). It represents a correlation space in which many quasars properties correlate with the optical Fe II strength (Boroson & Green 1992; Boroson 2002). EV1 is primarily governed by the black hole accretion process parameterized by the Eddington ratio (Boroson & Green 1992; Boroson 2002; Yuan & Wills 2003; Marziani et al. 2001; Shen & Ho 2014; Sun & Shen 2015). The correlation between mass ratio and accretion rate parameters seen in Figure 7 is largely due to this EV1 dependence.

Du et al. (2016, Figure 1) show the correlation between  $\mathcal{R}_{\text{Fe}}$  and  $L_{\text{Bol}}/L_{\text{Edd}}$  (also,  $\mathcal{M}$ ) for the SDSS DR5 sample of Hu et al. (2008) and RM AGNs. We plot versions of this correlation in Figure 11 for our low and high- $z$  samples. The left panel of Figure 11 demonstrates that using an underestimated Eddington ratio based on the canonical black hole mass ( $L_{\text{Bol}}/L_{\text{Edd}} \propto M_{\text{BH}}^{-1}$ ) gives a Pearson  $r$  correlation coefficient of only 0.31. The Fe-corrected black hole mass more accurately determines a higher Eddington ratio for the strong  $\mathcal{R}_{\text{Fe}}$  emitters, improving the correlation to  $r = 0.57$  (Figure 11, middle panel). The right panel of Figure 11 shows the strongest correlation,  $r = 0.61$ , between  $\mathcal{R}_{\text{Fe}}$  and Fe-corrected  $\mathcal{M}$ . We recognize that the much larger correlation coefficient is in part an effect of self-correlation induced by the addition of  $\mathcal{R}_{\text{Fe}}$  factor in the Du & Wang (2019) R-L relationship to estimate the Fe-corrected mass and consequently the Fe-corrected accretion rate parameters.

## 5 DISCUSSION

### 5.1 Selection biases and overall distribution of bright quasar properties

It is worth noting that the samples we use are not comprehensive and have selection effects. These samples, however, are likely representative of bright quasars at low and high redshifts and demonstrate the importance of the Fe-correction on the black hole mass estimates of highly accreting AGNs, especially at high-redshift.

The luminosities and redshifts of the quasars we use depend on various selection effects, such as adopted signal-to-noise ratio cuts and the wavelength of red-shifted H $\beta$  and if it falls in a spectral window observable from the ground, as well as the properties of the quasar population itself. For instance, there are no extremely luminous quasars at low-redshift, as only the lower mass objects are actively accreting, whereas at high redshift it is the most massive systems that are actively forming, a phenomenon known as “downsizing” (Heckman et al. 2004; Hasinger et al. 2005). To show these and other effects, we plot the mass-luminosity plane for all our samples in Figure 12. We see that there are quasars accreting at or slightly above the Eddington luminosity in both the low and high-redshift samples, but they are of intrinsically different masses and luminosity. Furthermore, it is only a small fraction of the low-redshift quasars that show such high accretion rates, as compared to the high-redshift samples. There are de facto luminosity cuts for the lowest mass black holes ( $< 10^8 M_{\odot}$ ), which must be accreting at Eddington ratios greater than  $\sim 0.1$  to be luminous enough to be included in the sample. The near-IR spectral surveys naturally chose the most luminous and highest accretion rate quasars with the largest black hole masses. There is also a de facto accretion rate limit below  $\sim 0.01$  of the Eddington ratio, where active galaxies stop displaying broad emission lines (e.g., Guolo et al. 2021, and references within).

Figure 13 plots our Fe-corrected black hole masses against our accretion rate indicators, and features a colour scheme to identify the values of  $\mathcal{R}_{\text{Fe}}$  across the plane. The super-Eddington accreting quasars in both low and high-redshift samples in general display the largest  $\mathcal{R}_{\text{Fe}}$  measurements. The quasars with large black hole masses and the lowest accretion rates in general display the smallest  $\mathcal{R}_{\text{Fe}}$  measurements. We show the distribution of  $\mathcal{R}_{\text{Fe}}$  in the low- $z$  and the combined high- $z$  samples in Figure 14. To illustrate the diversity in accretion rates of low- $z$  quasars, we further divided the low- $z$  sample into low and high mass. There are 692 out of 3309

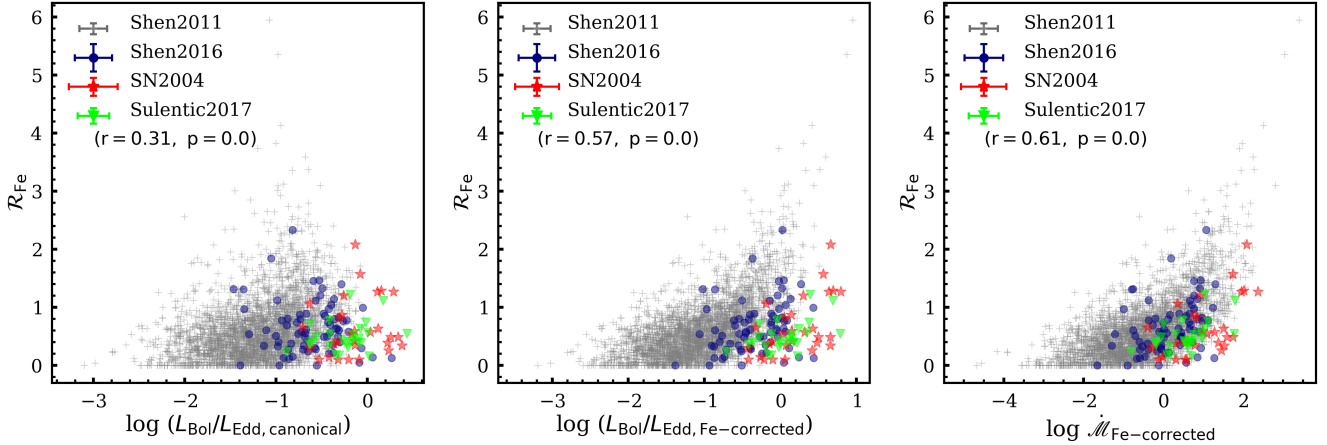


**Figure 11.**  $\mathcal{R}_{\text{Fe}}$  vs canonical Eddington ratio (left), Fe-corrected Eddington ratio (middle) and Fe-corrected  $\mathcal{M}$  (right). The Pearson correlation coefficients  $r$  and  $p$  are given in parentheses.

quasars in the low- $z$  sample with a mass less than  $10^8 M_{\odot}$ , while the remaining 79% have a mass  $\geq 10^8 M_{\odot}$ . We excluded 11 quasars in the low-mass low- $z$  sample (spectra shown in Appendix B) that have  $\mathcal{R}_{\text{Fe}} > 3$ . Figure 14 demonstrates that low mass, low- $z$  quasars have higher accretion rates (Figure 13) and stronger  $\mathcal{R}_{\text{Fe}}$  (Figure 14). They are the low mass analogs of massive highly accreting quasars at high- $z$ , albeit less massive and less luminous. On the other hand, the high-mass quasars in the low- $z$  sample have lower accretion rates and smaller  $\mathcal{R}_{\text{Fe}}$  measurements. The distribution of  $\mathcal{R}_{\text{Fe}}$  in the high- $z$  quasars shows that they consist of strong Fe II emitters and generally lack quasars with very small or zero  $\mathcal{R}_{\text{Fe}}$ .

## 5.2 Importance of the $\mathcal{R}_{\text{Fe}}$ correction

Two dimensionless quantities commonly used to parameterize the black hole’s accretion rate are Eddington ratio ( $L_{\text{Bol}}/L_{\text{Edd}}$ ) and  $\mathcal{M}$ . With the increasing number of RM measurements, many studies use these quantities to correct the R-L relationship for accretion-rate dependence. Fonseca Alvarez et al. (2020) point out that correlations between an  $R_{\text{BLR}}$  offset, i.e., the difference between  $R_{\text{BLR}}$  from RM measurement and one estimated from R-L relationship, and accretion rate estimators suffer from self-correlation. The  $R_{\text{BLR}}$  offset is proportional to the ratio of  $R/L^{0.5}$ ,  $L_{\text{Bol}}/L_{\text{Edd}} \propto L_{5100\text{\AA}}/R$  and  $\mathcal{M} \propto L_{5100\text{\AA}}^{1.5}/R^2$ . Therefore, using an independent estimate of accretion rate like  $\mathcal{R}_{\text{Fe}}$  is better. A strong anti-correlation is seen between the BLR size offset and  $\mathcal{R}_{\text{Fe}}$  for RM AGNs in the SEAMBH sample (Du et al. 2018; Du & Wang 2019). Grier et al. (2017), however, studied their H $\beta$  SDSS-RM sample and did not find this anti-correlation (Fonseca Alvarez et al. 2020). The H $\beta$  SDSS-RM sample has a median  $L_{\text{Bol}}/L_{\text{Edd}} \sim 0.1$  (Shen et al. 2019) and lacks extremely high accretors. For low-accreting AGNs, both accretion rate and, perhaps, black hole spin, govern the BLR size (Wang et al. 2014a; Du et al. 2018). After dividing the SDSS-RM sample into high and low accretion rate, Du et al. (2018) show that the high accretion rate sub-sample follows the expected anti-correlation between the BLR size offset and  $\mathcal{R}_{\text{Fe}}$  (see Figure 5 of Du et al. 2018).

Our results demonstrate the significant impact of including  $\mathcal{R}_{\text{Fe}}$  in the R-L relationship on the determination of black hole mass and accretion rate parameters. Such accretion rate-based correction is crucial for luminous broad-absorption line (BAL) quasars that are

known to have strong Fe II (Turnshek et al. 1997; Boroson 2002; Yuan & Wills 2003; Runnoe et al. 2013a, and references therein). We found that the strongest Fe-emitters in general have higher accretion rate, and consequently overestimated black hole mass. Quasars with  $L_{\text{Bol}}/L_{\text{Edd}} \geq 1$  can have black hole mass overestimated by up to an order of magnitude (as shown in Figure 7).

## 5.3 Some caveats for black hole mass estimation

We made some choices, depending on the availability of data, that impacted our results. Past studies interchangeably used flux ratio and EW ratio to define  $\mathcal{R}_{\text{Fe}}$ . To check how much this impacts estimates of black hole mass, we evaluated the change in  $\mathcal{R}_{\text{Fe}}$  by using each of these two quantities, in turn, to estimate black hole masses for the Shen et al. (2011) sample. They tabulate EWs of H $\beta$  and Fe II. We used the given EW and line luminosity for H $\beta$  to compute the continuum luminosity at 4861 Å. We scaled the continuum luminosity to the mean wavelength of Fe II i.e., 4560 Å using the slope for the H $\beta$  region and calculated the line luminosity for Fe II. The mean percentage difference between  $\mathcal{R}_{\text{Fe}}$  measured from line luminosity ratios and EW ratios is  $3.2 \pm 0.1\%$  and the standard deviation is  $\sim 4\%$ .

The FWHM and line dispersion,  $\sigma_{\text{line}}$ , both used as a proxy for velocity width in the virial mass formula, have their pros and cons. All the samples we used have available FWHM measurements of the H $\beta$  line as its measurement has been more common than  $\sigma_{\text{line}}$  in catalogs. FWHM is also less sensitive to line wings and blending with narrow lines (Peterson et al. 2004). But, for at least the radioloud subclass, FWHM is known to correlate with quasar orientation (Wills & Browne 1986). Dalla Bontà et al. (2020) show that for H $\beta$  both FWHM and  $\sigma_{\text{line}}$  provide reasonable proxies, with  $\sigma_{\text{line}}$  being slightly better. Some other investigations indicate that  $\sigma_{\text{line}}$  gives better virial mass estimates; for example, Peterson et al. (2004) find a tighter virial correlation when using  $\sigma_{\text{line}}$ , and Denney et al. (2013) find that H $\beta$  and C IV-based mass agree better when using  $\sigma_{\text{line}}$ . Collin et al. (2006) compare virial black hole mass based on different line-width measurements with black hole mass from the stellar velocity dispersion of RM AGNs. They find that the  $\sigma_{\text{line}}$ -based mass is better, albeit at low statistical significance. Recently, Wang et al. (2019) presented a similar study using the SDSS-RM quasars and reported that although FWHM suffers from orientation effects

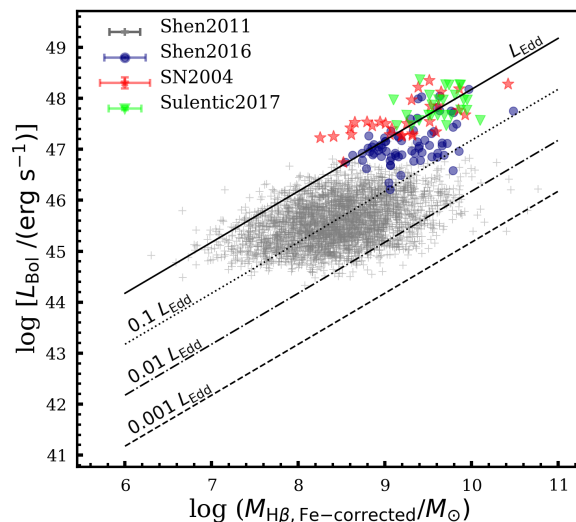


**Figure 12.** Bolometric luminosity vs Fe-corrected black hole mass for all samples. The black solid line represents the  $L_{\text{Bol}} = L_{\text{Edd}}$ , dotted line represents  $L_{\text{Bol}} = 0.1 L_{\text{Edd}}$ , dotted-dashed line represents  $L_{\text{Bol}} = 0.01 L_{\text{Edd}}$  and dashed line represents  $L_{\text{Bol}} = 0.001 L_{\text{Edd}}$ .

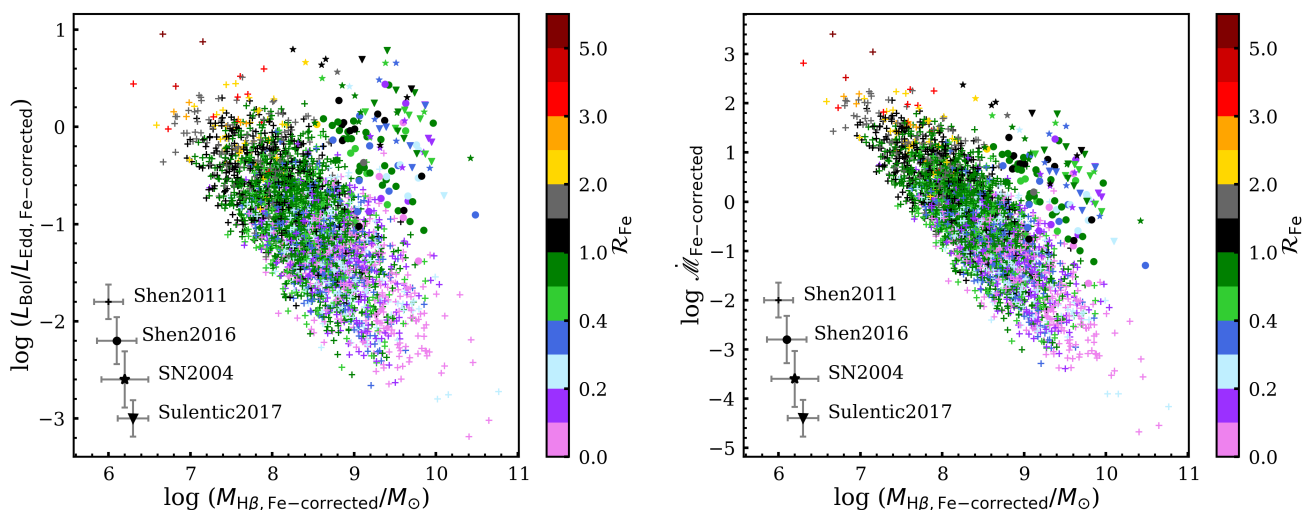


**Figure 13.** Fe-corrected mass vs accretion rate parameter colour-coded by  $\mathcal{R}_{\text{Fe}}$ .

more than  $\sigma_{\text{line}}$ , the use of  $\sigma_{\text{line}}$  does not guarantee a better virial mass estimate. An anti-correlation between FWHM and the virial coefficient is known, and using a constant value for  $f$  introduces additional uncertainty to the mass estimates (Mejía-Restrepo et al. 2018).

If the average viewing angle in the low- $z$  RM sample differs from that in luminous bright high- $z$  quasars, this could introduce an additional bias in the black hole mass estimates. The virial coefficient  $f$  very likely correlates with inclination angle (Pancoast et al. 2014; Collin et al. 2006).

A couple of possible competing orientation effects can introduce systematic biases that we may investigate in the future. For example, there is an observational bias due to the anisotropic nature of an accretion disk. The continuum emission varies with orientation (e.g., Runnoe et al. 2013c): a face-on disk is brighter than a relatively edge-on disk leading to a selection bias towards more face-on sources in luminous high- $z$  samples (DiPompeo et al. 2014). Although, if the selection is entirely random, we should observe more relatively edge-on sources because of the higher probability

of line of sight being edge-on than face-on. These factors must be considered along with the likelihood that AGN opening angles increase with increasing luminosity (e.g., Lawrence 1991; Ma & Wang 2013).

It is worth noting that the RM mass has an inherent uncertainty of 0.3-0.5 dex due to its calibration against the  $M - \sigma_{\star}$  relation (Peterson 2010; Vestergaard et al. 2011; Shen 2013; Ho & Kim 2014). The SE mass estimates have a 0.5-0.6 dex relative uncertainty and 0.7 dex absolute uncertainty (e.g., Table 5, Vestergaard & Peterson 2006).

Our updated SE mass prescription using the  $\mathcal{R}_{\text{Fe}}$ -based correction will not improve the precision of the estimate in individual objects, but will improve the accuracy, particularly for those with high accretion rates, which otherwise would be systematically over-estimated. While the correction will generally be smaller than the overall absolute uncertainty, correcting for systematic effects is important.

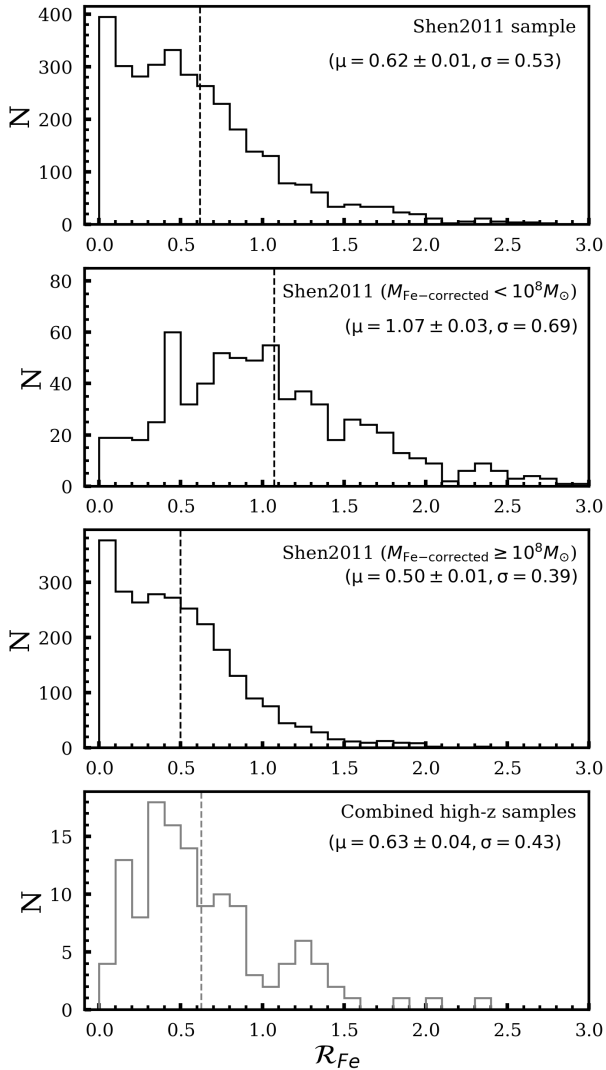


**Figure 14.** Distribution of  $\mathcal{R}_{\text{Fe}}$  in low-redshift sub-samples of Shen et al. 2011 (top three panels) and all the high-redshift samples combined together (bottom panel). The plot excludes targets with  $\mathcal{R}_{\text{Fe}} > 3$ .

## 6 CONCLUSIONS AND FUTURE OUTLOOK

The recently established R-L relation by Du & Wang (2019) takes into account the bias due to the accretion rate using  $\mathcal{R}_{\text{Fe}}$ . We use quasar samples across a wide range of redshifts from Shemmer et al. (2004), Netzer et al. (2004), Shemmer et al. (2010), Shen et al. (2011), Shen (2016) and Sulentic et al. (2017) to characterize the bias in black hole mass and accretion rate when using the canonical and Du & Wang (2019) R-L relationships. The single-epoch black hole mass estimates using the canonical R-L relationship systematically overestimate the mass of the black hole and underestimate the accretion rate. At high redshift, the black hole mass has likely been overestimated by a factor of two on average when using the canonical R-L relationship. The overestimation could be up to an

order of magnitude for the most highly accreting quasars, likely the most luminous such objects in the early universe. Our results also indicate that the high-redshift luminous quasars have highly accreting black holes whose optical spectra have characteristically strong  $\mathcal{R}_{\text{Fe}}$ . The low-redshift analogs of these highly accreting quasars are less massive but also exhibit strong  $\mathcal{R}_{\text{Fe}}$ . The use of the canonical R-L relationship results in an overestimation of black hole mass by a factor of two, on average, for both these highly accreting quasar populations.

The largest galaxy interactions/growth and star formation rates occur at cosmic noon, along with the most luminous quasars that will preferentially have very high accretion rates. Kelly & Shen (2013) show that the fraction of highly accreting AGNs increases with increasing redshift. The gas fraction in AGN host galaxies increases with redshift, likely contributing to the higher accretion rates (Shirakata et al. 2019). Hence, the mass and accretion rate corrections are relatively common among the most luminous quasars at cosmic noon, and likely the case at even higher redshifts. Low-accretion rate AGNs likely exist at these redshifts but are more commonly below the flux limits of surveys like SDSS, or only have low S/N spectra currently available (e.g., Kelly & Shen 2013).

In the absence of rest-frame optical spectra for high-redshift objects, Mg II and C IV provide an alternative for black hole mass estimation. Such mass estimates assume that the emission line follows normal “breathing”, i.e., as continuum luminosity increases, the time lag between continuum and emission-line variation increases, and the emission-line width decreases. Only the H $\beta$  line truly follows this; Mg II shows no breathing, whereas C IV shows anti-breathing (Wang et al. 2020). To correctly determine the black hole mass and accretion rate for high-redshift quasars, we need more near-IR spectroscopic surveys to facilitate direct checks using the H $\beta$  line. In the future, the Gemini Near-Infrared Spectrograph-Distant Quasar Survey (Matthews et al. 2021) will provide a large, uniformly distributed sample of quasars at high redshift. It will provide measurements of H $\beta$ , Fe II, [O III], and other UV lines that fall in the near-IR regions. The final data set will have a high signal-to-noise ratio (SNR $\sim$ 35) in the observed-frame  $\sim 0.8 - 2.5 \mu\text{m}$  band for a few hundred SDSS quasars at  $1.5 \leq z \leq 3.5$ . The wavelength coverage of the survey may enable the use of the C IV line and other UV features to determine an  $\mathcal{R}_{\text{Fe}}$  equivalent in the near-IR.

The presence of a billion solar mass quasar at  $z > 6$  is a problem because it is challenging to create and provide constant feeding of the black hole when the universe was less than a billion years old (Turner 1991; Haiman & Loeb 2001; Shen 2013; Inayoshi et al. 2020). Our results indicate that the black hole masses of high-redshift quasars are typically overestimated, especially for the most highly accreting black holes. Understanding the formation and evolution of massive black holes in the early universe necessitates taking into consideration  $\mathcal{R}_{\text{Fe}}$ -based accretion rate bias in their black hole mass estimates.

## ACKNOWLEDGEMENTS

We thank the anonymous referee for the constructive comments that improved the manuscript. JMW acknowledges support from the National Science Foundation of China (NSFC-11833008 and -11991054) and from the National Key R&D Program of China (2016YFA0400701). PD acknowledges the support from NSFC-11873048, -11991051 and the Strategic Priority Research Program of the Chinese Academy of Sciences (XDB23010400). This work

is supported by National Science Foundation grants AST-1815281 (O. S., B. M., C. D.) and AST-1815645.

#### DATA AVAILABILITY

The data underlying this article are available in Shen et al. 2011 (DOI: 10.1088/0067-0049/194/2/45), Shen 2016 (DOI: 10.3847/0004-637X/8171/1/55), Shemmer et al. 2004 (DOI: 10.1086/423607), Netzer et al. 2004 (DOI: 10.1086/423608), Sulentic et al. 2017 (10.1051/0004-6361/201630309), and Shemmer et al. 2010 (DOI: 10.1088/2041-8205/722/2/L152). See Section 3 for the sample selection criteria applied.

#### References

- Abazajian K. N., et al., 2009, *ApJS*, **182**, 543
- Bentz M. C., Katz S., 2015, *PASP*, **127**, 67
- Bentz M. C., Peterson B. M., Pogge R. W., Vestergaard M., Onken C. A., 2006, *ApJ*, **644**, 133
- Bentz M. C., Peterson B. M., Netzer H., Pogge R. W., Vestergaard M., 2009, *ApJ*, **697**, 160
- Bentz M. C., et al., 2013, *ApJ*, **767**, 149
- Blandford R. D., McKee C. F., 1982, *ApJ*, **255**, 419
- Boroson T. A., 2002, *ApJ*, **565**, 78
- Boroson T. A., Green R. F., 1992, *ApJS*, **80**, 109
- Brotherton M. S., Runnoe J. C., Shang Z., DiPompeo M. A., 2015, *MNRAS*, **451**, 1290
- Collin S., Kawaguchi T., Peterson B. M., Vestergaard M., 2006, *A&A*, **456**, 75
- Collinge M. J., et al., 2005, *AJ*, **129**, 2542
- Dalla Bontà E., et al., 2020, *ApJ*, **903**, 112
- Davies F. B., Hennawi J. F., Eilers A.-C., 2019, *ApJ*, **884**, L19
- Denney K. D., Peterson B. M., Dietrich M., Vestergaard M., Bentz M. C., 2009, *ApJ*, **692**, 246
- Denney K. D., Pogge R. W., Assef R. J., Kochanek C. S., Peterson B. M., Vestergaard M., 2013, *ApJ*, **775**, 60
- DiPompeo M. A., Myers A. D., Brotherton M. S., Runnoe J. C., Green R. F., 2014, *ApJ*, **787**, 73
- Du P., Wang J.-M., 2019, *ApJ*, **886**, 42
- Du P., et al., 2014, *ApJ*, **782**, 45
- Du P., et al., 2015, *ApJ*, **806**, 22
- Du P., Wang J.-M., Hu C., Ho L. C., Li Y.-R., Bai J.-M., 2016, *ApJ*, **818**, L14
- Du P., et al., 2018, *ApJ*, **856**, 6
- Fonseca Alvarez G., et al., 2020, *ApJ*, **899**, 73
- Grier C. J., et al., 2017, *ApJ*, **851**, 21
- Guolo M., Ruschel-Dutra D., Grupe D., Peterson B. M., Storchi-Bergmann T., Schimoia J., Nemmen R., Robinson A., 2021, *MNRAS*, **508**, 144
- Haiman Z., Loeb A., 2001, *ApJ*, **552**, 459
- Hasinger G., Miyaji T., Schmidt M., 2005, *A&A*, **441**, 417
- Heckman T. M., Kauffmann G., Brinchmann J., Charlot S., Tremonti C., White S. D. M., 2004, *ApJ*, **613**, 109
- Ho L. C., Kim M., 2014, *ApJ*, **789**, 17
- Hogg D. W., Baldry I. K., Blanton M. R., Eisenstein D. J., 2002, arXiv e-prints, [pp astro-ph/0210394](https://arxiv.org/abs/astro-ph/0210394)
- Hu C., Wang J.-M., Ho L. C., Chen Y.-M., Zhang H.-T., Bian W.-H., Xue S.-J., 2008, *ApJ*, **687**, 78
- Inayoshi K., Visbal E., Haiman Z., 2020, *ARA&A*, **58**, 27
- Johnson J. L., Whalen D. J., Fryer C. L., Li H., 2012, *ApJ*, **750**, 66
- Kaspi S., Smith P. S., Netzer H., Maoz D., Jannuzi B. T., Giveon U., 2000, *ApJ*, **533**, 631
- Kaspi S., Maoz D., Netzer H., Peterson B. M., Vestergaard M., Jannuzi B. T., 2005, *ApJ*, **629**, 61
- Kaspi S., Brandt W. N., Maoz D., Netzer H., Schneider D. P., Shemmer O., 2007, *ApJ*, **659**, 997
- Kaspi S., Brandt W. N., Maoz D., Netzer H., Schneider D. P., Shemmer O., Grier C. J., 2021, arXiv e-prints, [p. arXiv:2106.00691](https://arxiv.org/abs/2106.00691)
- Kelly B. C., Shen Y., 2013, *ApJ*, **764**, 45
- Kormendy J., Ho L. C., 2013, *ARA&A*, **51**, 511
- Laor A., 1998, *ApJ*, **505**, L83
- Lawrence A., 1991, *MNRAS*, **252**, 586
- Lodato G., Natarajan P., 2006, *MNRAS*, **371**, 1813
- Ma X.-C., Wang T.-G., 2013, *MNRAS*, **430**, 3445
- Martínez-Aldama M. L., Zajaček M., Czerny B., Panda S., 2020, *ApJ*, **903**, 86
- Marziani P., Sulentic J. W., Zwitter T., Dultzin-Hacyan D., Calvani M., 2001, *ApJ*, **558**, 553
- Marziani P., Sulentic J. W., Stirpe G. M., Zamfir S., Calvani M., 2009, *A&A*, **495**, 83
- Matthews B. M., et al., 2021, *ApJS*, **252**, 15
- McIntosh D. H., Rieke M. J., Rix H. W., Foltz C. B., Weymann R. J., 1999, *ApJ*, **514**, 40
- Mejía-Restrepo J. E., Lira P., Netzer H., Trakhtenbrot B., Capellupo D. M., 2018, *Nature Astronomy*, **2**, 63
- Mineshige S., Kawaguchi T., Takeuchi M., Hayashida K., 2000, *PASJ*, **52**, 499
- Mortlock D. J., et al., 2011, *Nature*, **474**, 616
- Netzer H., Peterson B. M., 1997, Reverberation Mapping and the Physics of Active Galactic Nuclei. p. 85, [doi:10.1007/978-94-015-8941-3\\_8](https://doi.org/10.1007/978-94-015-8941-3_8)
- Netzer H., Shemmer O., Maiolino R., Oliva E., Croom S., Corbett E., di Fabrizio L., 2004, *ApJ*, **614**, 558
- Onken C. A., Ferrarese L., Merritt D., Peterson B. M., Pogge R. W., Vestergaard M., Wandel A., 2004, *ApJ*, **615**, 645
- Pancoast A., Brewer B. J., Treu T., Park D., Barth A. J., Bentz M. C., Woo J.-H., 2014, *MNRAS*, **445**, 3073
- Peterson B. M., 1993, *PASP*, **105**, 247
- Peterson B. M., 2010, *IAU Symposium*, **267**, 151
- Peterson B. M., 2014, *Space Sci. Rev.*, **183**, 253
- Peterson B. M., et al., 2004, *ApJ*, **613**, 682
- Richards G. T., et al., 2006, *ApJS*, **166**, 470
- Runnoe J. C., Ganguly R., Brotherton M. S., DiPompeo M. A., 2013a, *MNRAS*, **433**, 1778
- Runnoe J. C., Brotherton M. S., Shang Z., DiPompeo M. A., 2013b, *MNRAS*, **434**, 848
- Runnoe J. C., Shang Z., Brotherton M. S., 2013c, *MNRAS*, **435**, 3251
- Shakura N. I., Sunyaev R. A., 1973, *A&A*, **500**, 33
- Shemmer O., Netzer H., Maiolino R., Oliva E., Croom S., Corbett E., di Fabrizio L., 2004, *ApJ*, **614**, 547
- Shemmer O., et al., 2010, *ApJ*, **722**, L152
- Shen Y., 2013, Bulletin of the Astronomical Society of India, **41**, 61
- Shen Y., 2016, *ApJ*, **817**, 55
- Shen Y., Ho L. C., 2014, *Nature*, **513**, 210
- Shen Y., Liu X., 2012, *ApJ*, **753**, 125
- Shen Y., Greene J. E., Strauss M. A., Richards G. T., Schneider D. P., 2008, *ApJ*, **680**, 169
- Shen Y., et al., 2011, *ApJS*, **194**, 45
- Shen Y., et al., 2015, *ApJS*, **216**, 4
- Shen Y., et al., 2019, *ApJS*, **241**, 34
- Shirakata H., Kawaguchi T., Oogi T., Okamoto T., Nagashima M., 2019, *MNRAS*, **487**, 409
- Sulentic J. W., Stirpe G. M., Marziani P., Zamanov R., Calvani M., Braito V., 2004, *A&A*, **423**, 121
- Sulentic J. W., Repetto P., Stirpe G. M., Marziani P., Dultzin-Hacyan D., Calvani M., 2006, *A&A*, **456**, 929
- Sulentic J. W., et al., 2017, *A&A*, **608**, A122
- Sun J., Shen Y., 2015, *ApJ*, **804**, L15
- Trakhtenbrot B., Volonteri M., Natarajan P., 2017, *ApJ*, **836**, L1
- Turner E. L., 1991, *AJ*, **101**, 5
- Turnshek D. A., Monier E. M., Sirola C. J., Espey B. R., 1997, *ApJ*, **476**, 40
- Vestergaard M., Peterson B. M., 2006, *ApJ*, **641**, 689
- Vestergaard M., Denney K., Fan X., Jensen J. J., Kelly B. C., Osmer P. S., Peterson B., Tremonti C. A., 2011, *PoS*, **NLS1**, 038
- Volonteri M., Silk J., Dubus G., 2015, *ApJ*, **804**, 148

- Wandel A., Peterson B. M., Malkan M. A., 1999, *ApJ*, 526, 579  
Wang J.-M., Szuszkiewicz E., Lu F.-J., Zhou Y.-Y., 1999, *ApJ*, 522, 839  
Wang J.-M., Du P., Li Y.-R., Ho L. C., Hu C., Bai J.-M., 2014a, *ApJ*, 792, L13  
Wang J.-M., et al., 2014b, *ApJ*, 793, 108  
Wang S., et al., 2019, *ApJ*, 882, 4  
Wang S., et al., 2020, *ApJ*, 903, 51  
Wang F., et al., 2021, *ApJ*, 907, L1  
Wills B. J., Browne I. W. A., 1986, *ApJ*, 302, 56  
Wisotzki L., Christlieb N., Bade N., Beckmann V., Köhler T., Vanelle C., Reimers D., 2000, *A&A*, 358, 77  
Yu L.-M., Bian W.-H., Wang C., Zhao B.-X., Ge X., 2019, *MNRAS*, 488, 1519  
Yu L.-M., Zhao B.-X., Bian W.-H., Wang C., Ge X., 2020a, *MNRAS*, 491, 5881  
Yu L.-M., Bian W.-H., Zhang X.-G., Zhao B.-X., Wang C., Ge X., Zhu B.-Q., Chen Y.-Q., 2020b, *ApJ*, 901, 133  
Yuan M. J., Wills B. J., 2003, *ApJ*, 593, L11  
van Groningen E., Wanders I., 1992, *PASP*, 104, 700

## APPENDIX A: SELECTION CRITERIA PRODUCING THE HIGH-Z SUB-SAMPLES

(i) Shen (2016) cataloged the properties of 74 quasars in the redshift range  $1.5 \leq z \leq 3.5$ . 60/74 targets are from Shen & Liu (2012) in the redshift range 1.5 to 2.2, and 14 new quasars at  $z \sim 3.3$  were added by Shen (2016). All targets were selected from the SDSS DR7 quasar catalog to have an  $S/N > 10$  in the C IV through the Mg II spectral regions. They excluded targets with broad absorption features or unusual continuum shapes. Such selection criteria at high redshift result in a sample of very luminous quasars, yet they demonstrate similar diversity in spectral features as seen in low- $z$  quasars (Shen & Liu 2012; Shen 2016). Figure 3 of Shen (2016) presents the median spectrum of these 74 quasars. The median spectrum shows broader H $\beta$  and H $\alpha$  lines characteristic of massive black holes as compared to the low- $z$  quasars. These quasars span nearly the entire range of  $\mathcal{R}_{\text{Fe}}$ , and follow the EV1 trends seen in the low- $z$  quasars (Shen 2016, Figures 7 & 8).

(ii) The SN2004 sample includes 29 quasars in the redshift range  $2 \leq z \leq 3.5$ . They selected luminous quasars ( $L \geq 10^{46} \text{ erg s}^{-1}$ ) with H magnitudes  $\leq 17$  allowing them to obtain high S/N IR spectra. These quasars had archival UV spectra including the N V and C IV emission lines without severe absorption. Their selection criteria also required the H $\beta$  line to be unaffected by atmospheric absorption in the IR bands. Shemmer et al. (2004) show the spectrum of these quasars in their Figures 1, 2 & 3. These high- $z$  quasars also follow the EV1 trend, in fact, they occupy the same region on the  $\mathcal{R}_{\text{Fe}}$  vs  $L_{\text{Bol}}/L_{\text{Edd}}$  plot as the narrow-line Seyfert 1 galaxies from Boroson & Green 1992 (Netzer et al. 2004, Figure 8).

(iii) Sulentic et al. (2017) selected 28 quasars from the magnitude-limited ( $m_B \approx 17.5$ ) Hamburg ESO survey (Wisotzki et al. 2000) with  $z > 1.4$  to allow observation of the C IV spectral region. They are high-luminosity ( $\log L_{5100\text{\AA}} > 46 \text{ erg s}^{-1}$ ) quasars with the H $\beta$  region properties reported by Sulentic et al. 2004, 2006; Marziani et al. 2009. Two quasars in Sulentic et al. (2017) are known to be gravitationally lensed, another is a mini-broad absorption line quasar, and two are weak-line quasars (WLQs).

## APPENDIX B: WEAK-LINE QUASARS

With the assumption that virial mass method holds true for WLQs, we show the effect of the Fe-correction on the determination of

their black hole mass. Our analysis includes four WLQs, two from Sulentic et al. (2017) and two from Shemmer et al. (2010).

We discussed the sample selection criterion of Sulentic et al. (2017) in Appendix A; their WLQs have redshifts 1.52 and 1.58. WLQs in the Shemmer et al. (2010) sample are at a redshift of 3.49 and 3.55 and were selected from Collinge et al. (2005) for near-IR spectroscopy as their H $\beta$  regions fall in the middle of the K band. These latter WLQs show weaker H $\beta$  lines (Shemmer et al. 2010, Figure 2) in comparison to high- $z$  quasars with similar luminosities, but have reliable measurements of the parameters used for black hole mass estimates (Shemmer et al. 2010). Shemmer et al. (2010) suggest the weakness of low and high-ionization emission lines is due to a gas deficiency in the BLR indicated by a low BLR covering factor rather than an effect of extreme accretion rate. The H $\beta$  lines in WLQs from Sulentic et al. 2017 are of normal strength.

After utilizing the Du & Wang (2019) R-L relationship, Figure B1 (left) shows that the two WLQs from Shemmer et al. (2010) sample have extreme accretion rates, and their mass overestimated by a factor of  $\sim 14$ . The two WLQs from Sulentic et al. (2017) show a mass overestimation of a factor of  $\sim 2.5$ . Although Fe-correction is crucial for all four WLQs as they have strong Fe II, the effect of Fe-correction is most extreme in the WLQs with weaker H $\beta$  lines ( $\mathcal{R}_{\text{Fe}} \propto 1/\text{EW H}\beta$ ) from Shemmer et al. (2010) in comparison to the WLQs from Sulentic et al. (2017). However, WLQs with weak H $\beta$  lines in Shemmer et al. (2010) have larger measurement uncertainties associated with their FWHM and EW of H $\beta$  measurements and hence larger measurement errors in masses. The mass ratio vs redshift plot (Figure B1 right) does not have a significant change in mean mass ratio in the redshift bin by the inclusion of just two WLQs. The mean mass differences are  $0.14 \pm 0.00$  dex for  $z < 1$ ,  $0.28 \pm 0.01$  dex for  $1 < z < 2$ ,  $0.30 \pm 0.02$  dex for  $2 < z < 3$  and  $0.45 \pm 0.07$  dex for  $z > 3$ .

## APPENDIX C: SDSS SPECTRA OF HIGHLY ACCRETING QUASARS IN SHEN ET AL. 2011

Table C1 lists the name, EW of H $\beta$ , EW of Fe II,  $\mathcal{R}_{\text{Fe}}$ , and log of mass ratio i.e.,  $\log(M_{\text{H}\beta, \text{canonical}}/M_{\text{H}\beta, \text{Fe-corrected}})$  of Shen et al. (2011) quasars that appear as outliers ( $\log$  of mass ratio  $> 1$ ) in Figures 7, 8 & 9. Figure C1 shows the SDSS spectra of these quasars arranged in descending order of mass ratio. SDSS J152350.42+391405.2 shows broad absorption line features.

This paper has been typeset from a  $\text{\TeX}/\text{\LaTeX}$  file prepared by the author.

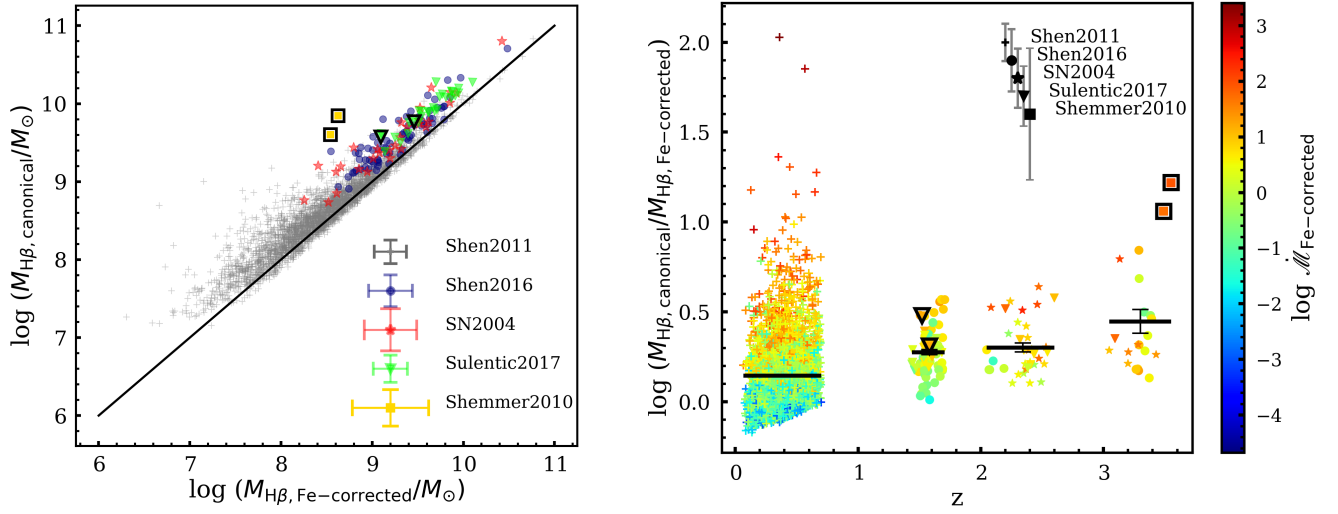


**Figure B1.** Left: Black hole mass calculated using the canonical (y-axis) and Fe-corrected (x-axis) R-L relations. Right: Mass ratio between canonical and Fe-corrected black hole mass vs redshift colour-coded by accretion rate. In both plots, WLQs are outlined in black.

**Table C1.** Outliers in Shen et al. (2011) sample

SDSSJ	$z$	EW(H $\beta$ ) ( $\text{\AA}$ )	EW(Fer1) ( $\text{\AA}$ )	$\mathcal{R}_{\text{Fe}}$	log(Mass ratio) (dex)
J140325.82+443014.1	0.4122	28.6	89.3	3.12	1.02
J094704.51+472142.8	0.5392	26.9	81.1	3.01	1.03
J131609.78-015403.9	0.4057	14.0	43.3	3.09	1.03
J093531.60+354101.0	0.4936	23.0	77.2	3.36	1.16
J104431.76+070841.0	0.6477	19.8	66.7	3.37	1.17
J224028.85-010649.8	0.1268	18.9	70.6	3.74	1.18
J152350.42+391405.2	0.6609	48.9	175.6	3.59	1.28
J130601.87+580319.9	0.4437	10.2	39.0	3.82	1.31
J092153.63+033652.6	0.3509	25.7	106.3	4.14	1.36
J083525.98+435211.3	0.5676	18.5	99.0	5.35	1.85
J131549.46+062047.8	0.3600	21.7	129.1	5.95	2.03

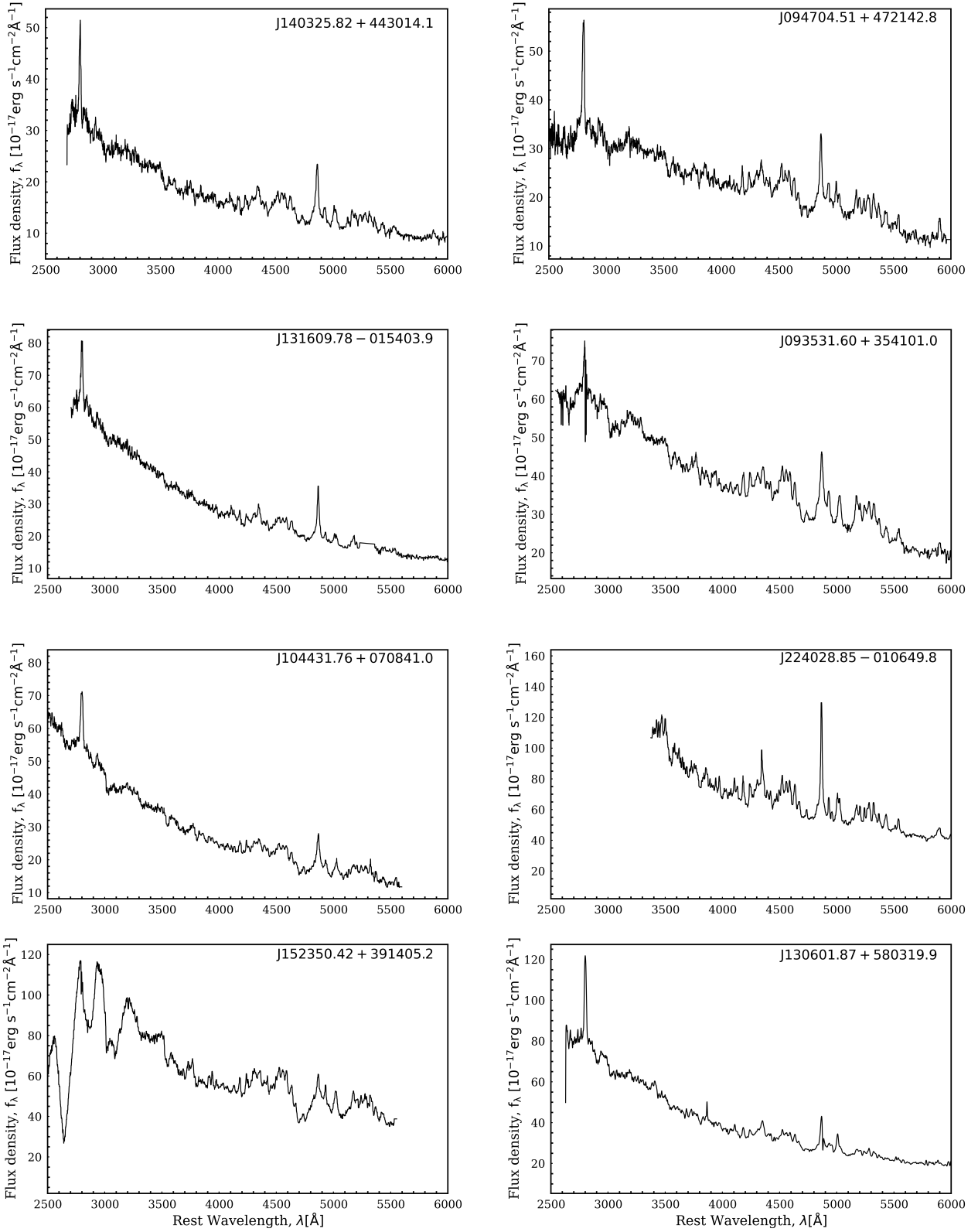
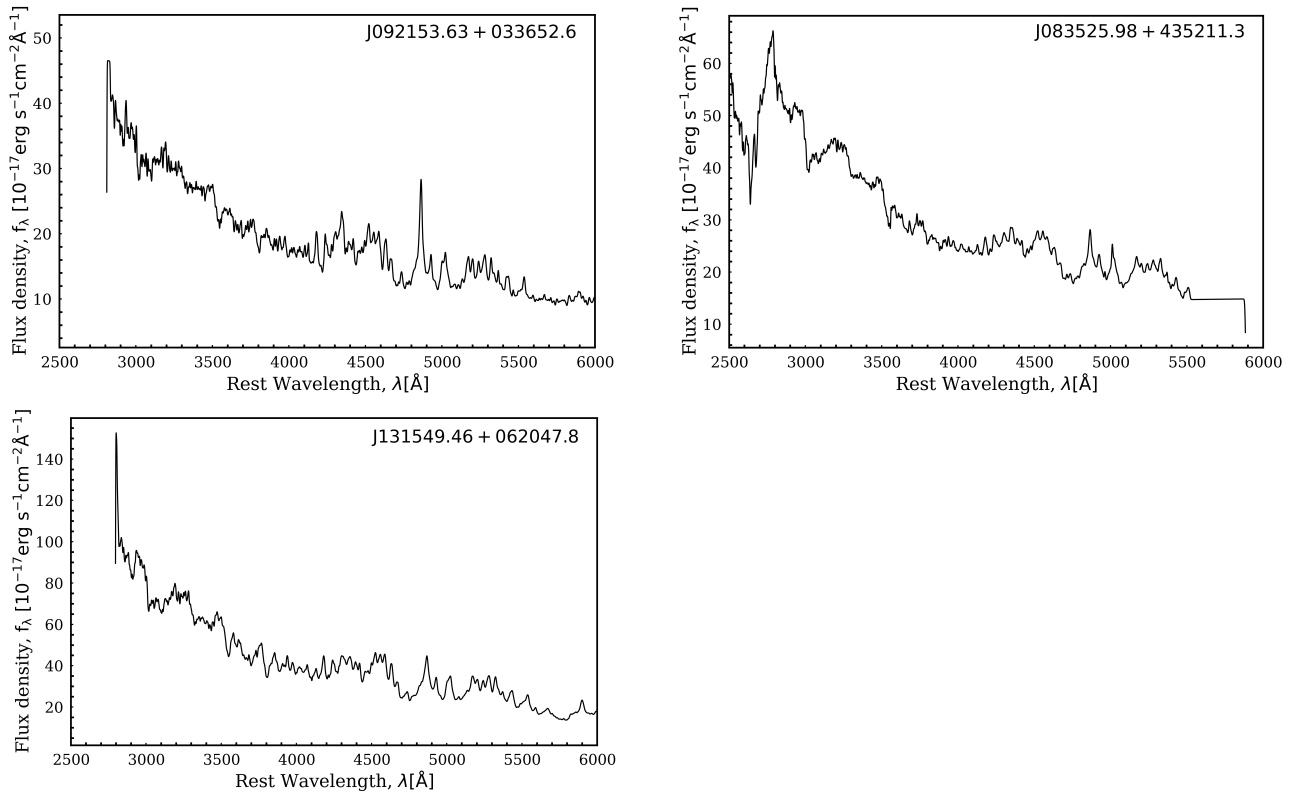


Figure C1. SDSS spectrum of outliers in Shen et al. (2011) sample. They have  $\mathcal{R}_{\text{Fe}} > 3$  and  $\log(M_{\text{H}\beta, \text{canonical}}/M_{\text{H}\beta, \text{Fe corrected}}) \geq 1$ .



**Figure C1** – *continued*